Cardiomyocyte differentiation from human induced pluripotent stem cells is delayed following knockout of Bcl-2

Tim Vervliet[1,*], Robin Duelen[2], Ankit Pradhan[3], Rita La Rovere[1], H. Llewelyn Roderick[3] and Maurilio Sampaolesi[2]

[1]Laboratory of Molecular and Cellular Signaling, Department of Cellular and Molecular Medicine, KU Leuven, 3000 Leuven, Belgium
[2]Translational Cardiomyology Laboratory, Department of Development and Regeneration, KU Leuven, 3000 Leuven, Belgium
[3]Laboratory of Experimental Cardiology, Department of Cardiovascular Sciences, KU Leuven, 3000 Leuven, Belgium

*Corresponding author: Tim Vervliet
Laboratory of Meolecular and Cellular Signaling, Department of Cellular and Molecular Medicine, KU Leuven, Campus Gasthuisberg, O&N I Herestraat 49 - bus 802, 3000 Leuven, Belgium
Email: tim.vervliet@kuleuven.be

Key words: Bcl-2; Ca^{2+} signaling; cardiomyocyte differentiation; human induced pluripotent stem cells

Summary statement

In this manuscript we address how Bcl-2 regulates the temporal trajectory of human induced pluripotent stem cell differentiation towards cardiomyocytes in a Myc dependent manner.

Abstract

Anti-apoptotic B-cell lymphoma 2 (Bcl-2) regulates a wide array of cellular functions involved in cell death, cell survival and autophagy. Less known is its involvement in the differentiation of cardiomyocytes. As a consequence, mechanisms by which Bcl-2 contributed to cardiac differentiation remain to be elucidated. To address this, we used CRISPR/Cas9 to knockout (KO) *BCL2* in human induced pluripotent stem cells (hiPSC) and investigated the consequence of this KO for

differentiation to cardiomyocytes. Our results indicate that differentiation of hiPSC to cardiomyocytes was delayed following *Bcl2* KO. This was not related to Bcl-2's canonical anti-apoptotic function. This delay lead to reduced expression and activity of the cardiomyocyte Ca^{2+} toolkit. Finally, Bcl-2 KO reduced c-Myc expression and nuclear localization in the early phase of the cardiac differentiation process, which accounts at least in part for the observed delay in the cardiac differentiation. These results propose a central role for Bcl-2 in cardiomyocyte differentiation and maturation.

Introduction

B-cell lymphoma 2 (Bcl-2) is involved in the regulation of cell death and survival decisions at multiple levels. Canonically, the anti-apoptotic Bcl-2 protein binds to pro-apoptotic Bcl-2-family members, such as Bax and Bak, thereby inhibiting their pro-apoptotic functions as inducers of mitochondrial outer membrane permeabilization (MOMP) and leading to cytochrome C release (Brunelle and Letai, 2009). In addition, Bcl-2 modulates inositol-1,4,5-trisphosphate receptors (IP_3R) thus, inhibiting pro-apoptotic Ca^{2+} signalling towards the mitochondria (Rong et al., 2008). Other Ca^{2+} handling proteins targeted by Bcl-2 include ryanodine receptors (RyR), sarco/endoplasmic reticulum ATPases and voltage dependent anion channels (Vervliet et al., 2016). Besides regulating the apoptotic outcome, Bcl-2 is involved in modulating autophagic flux. For instance, Bcl-2 associates with Beclin 1, thereby limiting the initiation of autophagosome formation and thus autophagic flux (Pattingre et al., 2005).

Regulation of cell death and survival is also key during differentiation. Consistently, Bcl-2 is involved in the differentiation of certain cells and tissues. For instance, neuronal differentiation has been shown to be regulated by Bcl-2. Transplanting embryonic stem cells overexpressing Bcl-2 in rat cortex enhanced recovery and neuronal differentiation after ischemic insult (Wei et al., 2005). In addition, overexpression of Bcl-2 in the PC12 neural crest tumour cell line, led to increased expression of genes associated with neural differentiation, whereas it decreased proliferation-related genes (Liang et al., 2003). In the heart, Bcl-2 was shown to be upregulated in a GATA4-dependent manner (Kobayashi et al., 2006), suggesting a role in cardiac development. The latter is further supported by the increased cardiomyocyte proliferation seen in mice overexpressing Bcl-2 in the heart (Limana et al., 2002). However, the molecular pathways underlying Bcl-2 regulation of cardiomyocyte differentiation remain uninvestigated.

Bcl-2 is phosphorylated at a number of sites resulting in modulation of its function. For example, Thr56, Ser70 and Ser87 located in the Bcl-2 unstructured loop are targets of multiple kinases including members of the mitogen-activated protein kinases (MAPK) family of kinases (Maundrell et

al., 1997, Blagosklonny, 2001, De Chiara et al., 2006). For example, phosphorylation of Bcl-2 by p38MAPK was demonstrated to induce apoptosis by inhibiting the anti-apoptotic function of Bcl-2 and inducing it to trigger the release of cytochrome C following MOMP induction in response to acute stressors (De Chiara et al., 2006). Phosphorylation of Bcl-2 has also been shown to result in its translocation to the nucleus (Zhou et al., 2017). In the nucleus, Bcl-2 interacts with c-Myc, increasing its stability and transcriptional activity (Jin et al., 2006). These functional interactions between Bcl-2, p38MAPK and c-Myc could also play a key role in the heart. Indeed, p38MAPK commits mouse embryonic stem cells to differentiate into cardiomyocytes (Aouadi et al., 2006) and regulates cardiomyocyte proliferation (Engel et al., 2005). Moreover, cardiac c-Myc overexpression in mice increases cardiac mass and hyperplasia without detrimental effects on cardiomyocyte maturation (Jackson et al., 1990).

In this study, we aim to further unravel the function of Bcl-2 in cardiomyocyte differentiation. To this end, we analysed the effect of CRISPR/Cas9-mediated *BCL-2* knock-out (KO) on the derivation of cardiomyocytes by differentiation from human induced pluripotent stem cells (hiPSC). We show that the temporal trajectory of hiPSC differentiation towards cardiomyocytes is delayed by *BCL-2* KO, which resulted in functional changes. Furthermore, we showed that Bcl-2 KO cells have reduced c-Myc expression and nuclear localization during early cardiomyocyte differentiation compared to control cells. Moreover, in control cells this increased c-Myc expression coincided with upregulation of Bcl-2 levels. Together, these results support a critical role for Bcl-2 in the generation of cardiomyocyte differentiation from hiPSC and suggest a role for it in the development of cardiomyocytes.

Results

Creation and validation of Bcl-2 KO hiPSC

BCL2 KO was performed in the commercially available Gibco™ Episomal hiPSC Line (A18945) using a CRISPR/Cas9 based approach. Single-guide RNAs (sgRNAs) were designed to induce Cas9-mediated double-stranded breaks (DSBs) in the genomic DNA of hiPSC. sgRNAs specificity and CRISPR/Cas9 DSB cutting were evaluated in HEK293T cells. The most promising *BCL2* targeting sgRNA, designed to target an early sequence in the *BCL2* gene, was selected. Cas9-mediated gene editing was performed via homology-directed repair, using a plasmid-based donor template with homology arms for the *BCL2* gene region of interest, flanking a GFP-Hygromycin-TK expressing cassette for selection. Stop codon introducing point mutations, inserting a premature stop codon in the *BCL2* gene were introduced in one of the homology arm regions, in order to introduce mutations in the *BCL2* gene.

After antibiotic selection and single cell colony isolation, the presence of the Hygromycin cassette at the correct genomic locus was validated. Next, the Hygromycin cassette was removed following PiggyBac excision and Fialuridine (FIAU) selection, resulting in completely gene-editing-free Bcl-2 KO hiPSC lines. Sequencing analysis of the *BCL2* gene confirmed CRISPR/Cas9-mediated alterations in the *BCL-2* gene. In figure 1, we restricted the validation to two clones, Bcl-2 KO1 and Bcl-2 KO2, which were used in this study. At the genomic level, all tested clones were characterized by a base pair deletion or frame shift mutation in the *BCL2* gene. The majority of the tested clones exhibited a deletion of 4 base pairs (Figure 1A), resulting in the introduction of three premature stop codons at the protein level (Figure 1B). Verification at the protein level via immunoblot showed the absence of endogenous Bcl-2 in both clones (Figure 1C), suggesting a complete knock-out of the *BCL2* gene. Finally, we screened for potential CRISPR/Cas9 off-target effects based on the sequence homology of the used sgRNAs (Figure 1D). In both clones no alterations near the potential off-target sites were detected, showing no unwanted Cas9-mediated DSB cuts.

Bcl-*2* KO does not inhibit but delays the induction of cardiac differentiation

After validation and selection of two Bcl-2 KO clones, we determined the effects of Bcl-2 KO on cardiomyocyte differentiation. The differentiation scheme utilized in this study is depicted in Figure 2A. A commercially cardiomyocyte differentiation kit, was utilized and resulted in the robust generation of cardiomyocyte cultures.

Consistent with the manufacturer's instructions using this protocol, large areas of spontaneously beating cardiomyocytes were observed as early as day 7 in the control differentiation. In the Bcl-2 KO clones, spontaneous beating was not seen until at least 9 days after the induction of differentiation. Moreover, the regions of spontaneously active cardiomyocytes were scarcer and smaller (see also figure 4A, B). This would suggest that Bcl-2 KO impacts cardiac differentiation. To investigate this further, we first assessed whether Bcl-2 KO resulted in impaired induction of expression of early and late cardiomyocyte differentiation markers (Figure 2B). In control and Bcl-2 KO conditions, RT-qPCR analysis revealed a decrease in expression of pluripotency markers upon differentiation as expected. mRNA expression of the mesodermal marker *BRACH,* indicative of mesoderm induction, occurred as anticipated on day 2 of differentiation for both control and KO conditions. Consistent with their expected upregulation during early cardiac differentiation, *NKX2.5* and *GATA4* were increased in expression at day 7 and remained elevated for the remainder of the control differentiation. However, in both Bcl-2 KO lines, *NKX2.5* and *GATA4* showed significantly lower expression levels at day 7, which for *NKX2.5*, but not for *GATA4,* recovered at 14 days of differentiation. A similar trend was

observed in two (*MYH6 and TNNI3*) out of three (*TNNT2*) tested late stage cardiomyocyte differentiation markers. This delaying of cardiomyocyte differentiation by Bcl-2 KO either suggested that that Bcl-2 was required for the efficient upregulation of cardiac differentiation markers or that Bcl-2 contributes to increasing/maintaining the number of differentiated cardiomyocytes, which in turn mediates the increased expression of these cardiac differentiation markers.

To further support these observations and show that KO of Bcl-2 does not impair cardiomyocyte differentiation from hiPSC cultures, cardiomyocytes were immunostained for cardiac troponin T (cTnT) after 14 days of differentiation. In both control and KO conditions, we were able to detect areas of cTnT staining (Figure 2C), supporting the observation that KO of Bcl-2 did not completely prevent the differentiation of cardiomyocytes from hiPSC.

Bcl-2 KO does not trigger cell death induction or changes in the induction of autophagy in hiPSC-derived cardiomyocytes

One explanation for the lower expression of cardiac progenitor and cardiomyocyte markers in the Bcl-2 KO conditions could be that loss of Bcl-2 resulted in increased cell death, leading to a lower number of differentiated cells and an impact on population measures of differentiation. This is plausible as Bcl-2 is known to play important functions in apoptosis and autophagy, two pathways that may control cell numbers.

Bcl-2 is a key anti-apoptotic protein, known to bind to and inhibit pro-apoptotic Bax and Bak, crucial for the execution of apoptosis. Therefore, KO of Bcl-2 may lead to increased apoptotic cell death. In order to address this, we performed immunoblot analysis in which we probed for poly ADP-ribose polymerase (PARP), which is cleaved by active caspase 3, an effector of apoptosis downstream of Bax/Bak activation. No difference in the ratio of the cleaved to total PARP was observed between control and Bcl-2 KO lines, indicating no increase in caspase 3 activity (Figure 3A). To further support this, a more quantitative method for determining the levels of cell death was performed. Bcl-2 KO and control conditions differentiated for 0, 7, 14 and 21 days were co-stained with NucView®488, propidium iodide and a cell permeable Hoechst to monitor caspase 3 activation, cell integrity and total nucleus count respectively. All these dyes when active/present in the cell bind to nuclear DNA allowing their quantification relative to the total nuclear fluorescence of the Hoechst stain. Cells that were positive for either NucView®488 or NucView®488 together with propidium iodide were classified as apoptotic, whereas cells positive for propidium iodide only, were classified as necrotic. For each day of experiments a staurosporine treated control condition was used to set the threshold for cells being positive for NucView®488 and propidium iodide staining. Representative images for

each differentiation day and the tested conditions can be found as supplemental figure S1-4. Quantifying these experiments showed no significant differences in basal levels of either apoptosis or necrosis between control and Bcl-2 KO conditions (Figure 3B), confirming the PARP findings in figure 3A. Of note, early in the differentiation (day 7) there appeared to be more necrosis in all conditions compared to later stages of differentiation (day 14 and 21) where apoptosis induction was more pronounced.

Bcl-2 also plays important roles in the regulation of autophagy. By binding to Beclin 1 for instance, Bcl-2 impairs the induction of autophagosome formation thus potentially inhibiting autophagy induction. In order to measure autophagy induction, we monitored the levels of lipidated microtubule-associated protein light chain 3 (LC3-II). No difference in LC3-II levels could be detected between control and Bcl-2 KO clones (Figure 3C). In addition, we also monitored mammalian target of rapamycin (mTOR) activity by determining the phosphorylation state/activity of p70 S6 kinase (figure 3C), a downstream target of mTOR. Similar to the LC3-II results, the phosphorylation state of p70 S6 kinase was unaltered, confirming that Bcl-2 KO did not alter basal autophagic induction.

Finally, we validated whether the Bcl-2 KO clones could upregulate the closely related anti-apoptotic Bcl-X_L protein to compensate for the loss of Bcl-2. However, Bcl-X_L levels were not significantly altered in the Bcl-2 KO clones compared to the control and even seemed to decrease in all conditions rather than increase during differentiation (Figure 3C).

Bcl-2 KO reduces the area of beating cells and inhibits the amplitude of spontaneous Ca^{2+} transients in hiPSC-derived cardiomyocytes

As the induction of cardiomyocyte differentiation was delayed upon KO of Bcl-2 and no differences were observed in apoptosis and autophagy induction, we next examined whether functional measures of cell physiology were similarly affected in Bcl-2 KO hiPSC-derived cardiomyocytes. To these ends, we investigated spontaneous Ca^{2+} transients, which are responsible for the spontaneous contractions in control and Bcl-2 KO cardiomyocytes, using live cell Ca^{2+} imaging. Ca^{2+} imaging experiments were performed in cardiomyocytes differentiated for 9 or 11 days. At these time points it was feasible to detect spontaneously contracting areas in both control and Bcl-2 KO cardiomyocytes. Fluo-4 loading allowed the measuring of the surface area of beating cells by monitoring spontaneous changes in cytosolic [Ca^{2+}]. This analysis was visualised in Figure 4A as maximum intensity Z projections of the first 30 sec (300 images) of example control and Bcl-2 KO conditions. Compared to that observed in controls, the area of spontaneously active cardiomyocytes was severely decreased in Bcl-2 KO cells (Figure 4B). Next, we focused on the properties of the Ca^{2+}

changes. To assess the dynamics of Ca^{2+} transients over the image, pseudo-line scans of the largest area of spontaneously active cells were performed that spanned the duration of the experiment (Figure 4C). These analyses were performed by "reslicing" the entire stack time series over a vertical line in the image (the arrows in Figure 4A indicate where these lines were drawn) to generate an xt image. From this line stack, fluorescence intensity measurements were made and plotted as normalised fluorescence (F/F0). This was performed either for the entire slice area (black vertical bar Figure 4C) or was focussed on the area with the largest response (red bar, Figure 4C). A representative image of such a line stack for control and Bcl-2 KO clones can be seen in figure 4C. The intensity plot of the corresponding line stacks is shown in figure 4D. These analyses showed that Bcl-2 KO did not alter the frequency of the spontaneous Ca^{2+} release events compared to the control (Figure 4E). However, the amplitude (Figure 4F) and area under the curve (AUC; Figure 4G) were significantly lower in Bcl-2 KO cardiomyocytes, when quantifying the entire line stack. From figure 4A, B and the line stack, a larger area of control cardiomyocytes exhibited spontaneous activity compared to the Bcl-2 KO clones. Therefore, we also performed the same quantification but restricted the analysis to the major sites of cell activity (red line Figure 4C) and saw that both amplitude and AUC were no longer significantly different between control and Bcl-2 KO. These results confirmed that KO of Bcl-2 did not impair but rather delays cardiomyocyte differentiation from hiPSC. These data highlight the advantage of performing imaging experiments in which cell populations of differing maturation can be discretely analysed.

Bcl-2 KO impairs the expression of the cardiac Ca^{2+} toolkit

Our findings suggest that Bcl-2 KO delayed differentiation of hiPSC to cardiomyocytes and as a consequence spontaneous Ca^{2+} transients and contraction was inhibited. However, where Bcl-2 KO cells did differentiate they showed similar functional activity compared to controls. This suggests that Bcl-2 did not block cardiomyocyte differentiation per se but rather intervened in the decision as to whether hiPSC differentiate to cardiomyocytes or not. Given the association between the expression of specific Ca^{2+} handling machinery involved in excitation contraction coupling with cardiomyocyte maturation, we next investigated the underlying mechanisms for this reduced Ca^{2+} signalling capacity. To this end, immunoblot assays were performed to evaluate the expression levels of a number of proteins involved in cardiac function and Ca^{2+} handling (Figure 5). From these immunoblots it is clear that the expression levels of RyR2, the sodium Ca^{2+} exchanger (NCX), the cardiac specific sarco/endoplasmic reticulum ATPase 2A (SERCA2a) isoform and cardiac cTnT were dramatically lower in Bcl-2 KO cardiomyocytes compared to control cardiomyocytes. Inositol 1,4,5

trisphosphate receptor type 2 (IP_3R2) levels showed a similar decline in control and Bcl-2 KO conditions, indicated that the decrease is specific for cardiac specific markers. These results suggest that when examining the entire cell population in the Bcl-2 KO cultures, only a minority was fully differentiated to cardiomyocytes.

Bcl-2 KO impairs early c-Myc upregulation thereby resulting in reduced functional cardiomyocyte growth

KO of Bcl-2 did not alter the levels of apoptosis or basal autophagy induction. Besides participating in pathways involved in cell removal, Bcl-2 is also involved in the regulation of cellular proliferation differentiation and growth. An interesting link between Bcl-2 and c-Myc has been described whereby Bcl-2 would stabilize c-Myc thus increasing its expression and activity (Jin et al., 2006). To explore this possibility in hiPSC-derived cardiomyocytes, we determined c-Myc levels between control and Bcl-2 KO lines (Figure 6A). Interestingly, on differentiation day 7, c-Myc is upregulated in control cells, which was not the case in both Bcl-2 KO conditions. A similar non-significant trend was observed at day 14, whereas at day 21 c-Myc expression recovered to control levels. This observation suggests that loss of Bcl-2 resulted in decreased c-Myc expression during early cardiomyocyte differentiation from hiPSC.

It has been shown that phosphorylation of Bcl-2 by MAPK, a kinase heavily involved in regulating cell proliferation, leads to the nuclear translocation of Bcl-2 where it provides pro-survival signalling and chemoresistance (Zhou et al., 2017). This effect of Bcl-2 could at least be in part due to its stabilizing effects on c-Myc in the nucleus thus promoting c-Myc signalling (Jin et al., 2006). To validate the involvement of this pathway here, we determined levels of the active phosphorylated form of p38MAPK and of phosphorylated Bcl-2 by immunoblot analysis (Figure 6B). Levels of phosphorylated active p38MAPK relative to total p38MAPK levels were not altered between non-differentiated control and Bcl-2 KO cells. However, during differentiation p38MAPK expression levels significantly increased in control cardiomyocytes signifying an increase in absolute levels of phosphorylated p38MAPK. No such increase was detected during the differentiation of the Bcl-2 KO cells. Similarly, Bcl-2 phosphorylated at serine 70, a known target of MAPK pathways and which facilitate its nuclear translocation (Zhou et al., 2017), was upregulated together with total Bcl-2 throughout the differentiation of control hiPSC (Figure 6B). This quantification showed that relative to total Bcl-2 levels, no increase could be observed in Bcl-2 phosphorylation status. However, since both phosphorylated and total Bcl-2 levels clearly increased over time, it can be concluded that the absolute levels of phosphorylated Bcl-2 do increase. Interestingly, in the cardiomyocytes derived

from control hiPSC, Bcl-2 levels were upregulated from day 7 onward coinciding with the increased levels/activity of p38MAPK and c-Myc, highlighting the importance of Bcl-2 for cardiac differentiation.

The above results are in accordance with literature describing a stabilizing effect of Bcl-2 on c-Myc expression in the nucleus, which in turn allows efficient regulation of c-Myc dependent genes (Jin et al., 2006). In order to further validate whether this is also the case in our cardiomyocyte differentiations, immunofluorescence experiments were setup to determine whether the nuclear c-Myc levels were diminished following Bcl-2 KO (Figure 7). Since the largest differences in c-Myc expression were observed at day 7, we focused these experiments on this day. Control and Bcl-2 KO cardiomyocytes differentiated for 7 days were fixed and stained for c-Myc, cTnT and Hoechst (Figure 7A). Combing the Hoechst and c-Myc staining, the intensity and area occupied by c-Myc in the nucleus was quantified (Figure 7B). From this analysis, it was clear that both the intensity and area occupied by c-Myc in the nucleus were significantly decreased in Bcl-2 KO condition compared to control. cTnT stain was also imaged to illustrate that cardiac differentiation had started as is expected at day 7.

Overall, these results suggest that Bcl-2 KO reduced expression of c-Myc in the erly phase of cardiomyocyte differentiation and more specifically lowers the abundance of nuclear c-Myc. As c-Myc is an important regulator of the expression of genes involved in cardiomyocyte differentiation this may contribute to the delays in the differentiation observed in the Bcl-2 KO hiPSC-derived cardiomyocytes.

Discussion

In this study, we showed that Bcl-2 plays an important part in the early phase of cardiomyocyte differentiation from hiPSC. KO of Bcl-2 did not induce apoptosis or alter autophagic flux induction, but instead, resulted in delayed differentiation of cardiomyocytes from hiPSC. Our data point towards a role for Bcl-2 in regulating early c-Myc stability, a transcription factor known to be required for cardiac differentiation and growth (Jackson et al., 1990).

It is known that Bcl-2 plays important roles during differentiation of neurons and cardiomyocytes, although the involved pathways remain to be fully elucidated (Liang et al., 2003, Limana et al., 2002, Kobayashi et al., 2006, Wei et al., 2005). In this study, we aimed to address this further and build on known functions of Bcl-2 in cardiomyocyte differentiation. To this end, a CRISPR/Cas9-mediated knock-out of Bcl-2 was generated in hiPSC (Figure 1). The CRSIPR/Cas9 assay was intended to

introduce specific point mutations via homologous recombination in the *BCL2* gene, resulting in the introduction of a premature stop codon to prevent protein translation. Insertion of the selection cassette, that contained the mutations in the homology arm regions, was successful at the intended locus. However, after removal of the selection cassette none of the tested clones showed the introduction of the intended mutations. Rather, the majority of the clones showed a 4 base pair deletion at the sgRNA cut site, resulting in a frame shift and introduction of three premature stop codons, which effectively resulted in knocking-out Bcl-2. The lack of protein was confirmed by immunoblot, which showed a complete KO of Bcl-2 compared to the control line, indicating that these clones were suitable for use in this study.

After validating the KO of Bcl-2, the effects of lack of Bcl-2 on cardiomyocyte differentiation were addressed. In our differentiation of hiPSC to cardiomyocytes, no change in expression of pluripotency or mesoderm markers were detected between conditions suggesting Bcl-2 KO but also the CRISPR/Cas9 editing did not have an impact on the early stages of the differentiation. However, a delay in the expression profile of four out of five tested early and late markers of cardiomyocyte differentiation was observed in Bcl-2 KO compared to controls (Figure 2). This suggests that KO of Bcl-2 delays the differentiation of cardiomyocytes from hiPSC at later stages in the differentiation and not by halting mesoderm induction. This conclusion was further supported by data from experiments in which we recorded spontaneous intracellular Ca^{2+} release. The occurrence, frequency and properties of these events are used as an index of cardiomyocyte differentiation and maturation (Figure 4). From these experiments it was clear that control cardiomyocytes showed increased spontaneous Ca^{2+} release over larger areas compared to the Bcl-2 KO conditions. However, when focused exclusively on the major regions of activity no significant functional differences in the properties of the Ca^{2+} transients between control and Bcl-2 KO conditions could be detected. These results suggest that KO of Bcl-2 does not impair cardiomyocyte differentiation but rather influences the number of cells that successfully differentiate. This also fits well with the observation that Bcl-2 KO delays differentiation, which in turn limits the number of functional cardiomyocytes during the early stages of differentiation. A consideration here is that we are likely underestimating the effects of Bcl-2 KO on Ca^{2+} signalling as in these experiments, the decision to measure an area was made based on the presence of visual spontaneous activity. This spontaneous activity was much more pronounced in the control cardiomyocytes compared to the Bcl-2 KO. As such, in the Bcl-2 KO we are likely sampling the subpopulation of the cells that differentiated properly, did not show large defects when specifically analysed.

The latter is further confirmed by the lack of expression of critical members of the cardiac Ca^{2+} toolkit in Bcl-2 KO cardiomyocytes (Figure 5). These immunoblots monitor the average of the entire differentiating population. Based on the largely absent RyR, cTnT, SERCAa1 and NCX in the Bcl-2 KO conditions, it could be expected that no spontaneous activity would be detected in the Bcl-2 KO lines. Nevertheless, a subpopulation of these cells was still able to produce spontaneous Ca^{2+} reactivity and contractions (Figure 4). Furthermore, Bcl-2 KO did not result in excessive induction of apoptosis or changes in autophagic flux (Figure 3). Taken together, these results indicate that Bcl-2 KO delayed differentiation thereby limiting the number of functional cardiomyocytes without affecting their viability. This observed delay in differentiation might be a more general function of Bcl-2, not only restricted to cardiomyocytes, as Bcl-2 KO mice have severe growth retardation, which may be attributed to a general delay in differentiation when Bcl-2 is not present (Veis et al., 1993).

During cardiomyocyte differentiation, both p38MAPK and c-Myc activity play important roles in differentiation and growth. p38MAPK has been shown to act as a switch deciding between proliferation and differentiation of cardiomyocytes (Engel et al., 2005, Aouadi et al., 2006, Romero-Becerra et al., 2020). c-Myc expression in cardiomyocytes on the other hand is involved in cardiac growth (Jackson et al., 1990). Bcl-2 interacts with nuclear c-Myc thereby regulating its transcriptional activity and stability (Jin et al., 2006). Bcl-2 translocation to the nucleus is dependent on its phosphorylation status (Zhou et al., 2017). p38MAPK phosphorylates Bcl-2 facilitating its translocation towards the nucleus (De Chiara et al., 2006). Other MAPK also phosphorylate Bcl-2. ERK1/2 for instance phosphorylates Bcl-2 at Ser70 thereby impacting its anti-apoptotic functions (Deng et al., 2000) and its functional cooperation with c-Myc (Jin et al., 2004), suggesting this is an important mechanism for several MAPK in the regulation of Bcl-2. Our results show that p38MAPK is active and able to phosphorylate its targets before and during differentiation of both control and Bcl-2 KO conditions (Figure 6B). Under control conditions, Bcl-2 was phosphorylated and upregulated as has been previously described (Kobayashi et al., 2006). Together with Bcl-2, c-Myc levels were significantly higher at day 7 in control compared to KO conditions (Figure 6A, B). Prolonged differentiation resulted in recovery of c-Myc levels towards control levels in both KO lines. Looking more closely at the localization of c-Myc at day 7 revealed that c-Myc levels in the nucleus were reduced in the Bcl-2 KO conditions compared to controls (Figure 7). Since c-Myc positively regulates the expression of many genes (Patel et al., 2004), it is logical to deduce that reducing c-Myc levels would result in a reduction of c-Myc driven transcription and in turn reduced cardiac differentiation. Recently, it was shown that the transcriptional output of c-Myc in the heart, following upregulation of c-Myc, is largely dependent on the presence of transcriptional cofactors that determine which genes will be activated (Bywater et al., 2020). In our hands, we demonstrated a reduction in the

abundance of c-Myc upon Bcl-2 KO, suggesting that the lack of cofactors would not be an issue in this setting. However, in the context of cardiac differentiation of the Bcl-2 KO hiPSC, these cardiac specific cofactors are expected to direct the limited amount of c-Myc towards genes necessary for differentiation, thereby allowing this process to occur at a slow/delayed rate compared to that in the control condition. The low amount of c-Myc still available in the Bcl-2 KO conditions may at least in part explain the delay, and not a complete halt, in differentiation observed upon Bcl-2 KO.

In summary, our results indicate that Bcl-2 is required for maintaining the temporal trajectory of early cardiomyocyte differentiation by regulating c-Myc expression/localization to the nucleus. Given the importance of c-Myc for cardiac differentiation, in combination with the lack of effect of Bcl-2 KO on expression of pluripotency markers and mesoderm induction, we propose that this Bcl-2 dependent decline in c-Myc dysregulated the expression of cardiac specific genes. Loss of Bcl-2 resulted in delayed differentiation of cardiomyocytes from hiPSC by lowering nuclear c-Myc signalling. This results in less efficient accumulation of functional cardiomyocytes.

Materials and methods

Reagents and antibodies

Unless otherwise specified, all chemicals were purchased from Merck (Hoeilaart, Belgium). Primary antibodies were anti-Vinculin (#V-9131), anti-c-Myc (#M4439, Merck), anti-Tubulin (#556321, BD Pharmingen, Erembodegem, Belgium) anti-Bcl-2 (#sc7382HRP), anti-phospho Ser70-Bcl-2 (#sc-293128, Santa Cruz, Heidelberg, Germany), anti-phospho-p70 S6 kinase (#9234S), anti-p70 S6 kinase (#9202), anti-phospho-p38MAPK (#9215S), anti-p38MAPK (#9212), anti-Bcl-X_L (#2764), anti-PARP (#9532S, Cell Signalling, Leiden, The Netherlands), anti-LC3 (#0231-100/LC3-5F10, Nanotools, Teningn, Germany), Anti-RyR (C3:33) (#MA3-916), anti-NCX (#MA3-926, ThermoFisher Scientific, Waltham, MA, USA), anti-cTnT (#ab209813, Abcam, Cambridge, United Kingdom), anti-IP_3R2 (# R2872-2, Abiocode, Agoura Hills, CA, USA) and anti-SERCA2a (produced and kindly gifted by Prof. F. Wuytack (KU Leuven)). More information concerning antibody dilution and validation/references can be found in supplemental table S1. All primers and gene blocks used in this study were purchased from integrated DNA technologies (IDT; Leuven, Belgium). Primers were listed in (Supplemental table S2 and S3).

hiPSC culturing

All experiments were performed using the commercially available Gibco™ Episomal hiPSC Line (A18945; Thermo Fisher Scientific) which was regularly tested for presences of mycoplasma. hiPSC were cultured feeder-free on Geltrex LDEV-Free hESC-Qualified Reduced Growth Factor Basement Membrane Matrix (ThermoFisher; #A1413201) and maintained in Essential 8 Flex Basal Medium supplemented with Essential 8 Flex Supplement (50x) and 0.1% Pen/Strep (all from Thermo Fisher Scientific), at 37°C under normoxic conditions (21% O_2 and 5% CO_2). Medium was changed daily. Colonies were routinely passaged non-enzymatically with 0.5 mM EDTA in Phosphate-Buffered Saline (PBS) (Thermo Fisher Scientific).

Cardiomyocyte differentiation of hiPSC

For inducing cardiac differentiation, the iPSC cardiomyocyte differentiation kit (Thermo Fisher Scientific; #A2921201) was used according to the manufacturers protocol. Briefly, prior to differentiation, hiPSC were seeded on a thin Matrigel™ Growth Factor Reduced (GFR) Basement Membrane Matrix layer (Merck; #CLS356252) and cultured for 3 days in Essential 8 medium at 37°C under hypoxic conditions (5% O_2 and 5% CO_2) until the cells reached approximately 60% of confluency. Cardiomyocyte differentiation was started after the addition of a mesoderm-inducing medium (medium A; day 0) for 48 h. After 24 h, cells were transferred from hypoxia to normoxia. At day 2 of differentiation, cells were incubated for another 48 h with a cardiomyocyte progenitor medium (medium B). From day 4 onwards, medium was changed every other day with a cardiomyocyte maintenance medium. All experiments performed were approved by the Research Ethical Committee of UZ/KU Leuven (protocol number S62524).

Cloning of gRNA and selection plasmid

The *BCL2*-targeting sgRNA (forward: 5'-GAGAACAGGGTACGATAACC-3' and reverse: 5'-GGTTATCGTACCCtGTTCTC-3') was cloned in the pU6-(BbsI)CBh-Cas9-T2A-mCherry, a gift from Ralf Kuehn (Addgene plasmid # 64324 ; http://n2t.net/addgene:64324 ; RRID:Addgene_64324) (Chu et al., 2015), using the BbsI restriction enzyme. In order to introduce a hygromycin selection cassette into the genomic *BCL2* sequence, two genomic DNA sequences, in close proximity and on either side of a TTAA sequence within 500 bp of the *BCL-2* sgRNA, were identified. These sequences (one 430 bp (HAL sequence (see Supplemental table S4) and a 450 bp long (HAR sequence)) were introduced using the NEBuilder® HiFi DNA Assembly Master Mix (New England BioLabs) in combination with the sequences produced as gene blocks (IDT) and the PiggyBAC-Hygro-TK vector flanking the Hygromycin

resistance gene restricted with BamHI enzyme. In the HAR sequence, containing the start of the *BCL2* open reading frame, base pair substitution was incorporated in order to generate premature stop codons in the *BCL2* gene resulting in the knock-out.

CRISPR/Cas9-mediated knock-out of *BCL2*

Transfection of hiPSC was performed by nucleofection using the commercially available Cell Line Nucleofector Kit (Lonza) according to their protocol. For the nucleofection, 2 µg of the sgRNA containing plasmid and 8 µg of the selection plasmid were utilized. After nucleofection, the hiPSC were plated onto Geltrex coated culture plates. On the third day after nucleofection, 50 ng/ml Hygromycin was added to the medium to start the selection procedure. After 7 days of selection, single colonies were picked. The medium was refreshed each day with Essential 8 medium containing 50 ng/ml Hygromycin until the colonies were sufficiently grown, after which cells were passaged. At this point, a fraction of the hiPSC was taken for genomic DNA isolation to screen for the insertion of the Hygromycin selection cassette at the correct locus in the *BCL2* gene (see Supplemental table S2). Finally, in clones selected based on correct insertion of the Hygromycin gene in the *BCL2* locus, the selection cassette was again removed. To this end, hiPSC were detached and nucleofected with 5 µg of the PiggyBac transposase plasmid (kind gift of Prof. C. Verfaillie (KU Leuven)). The medium was changed daily using Essential 8 medium until cells reached 90% confluency. At this point Fialuridine (FIAU; Merck) selection was started for 24 h to kill cells in which the selection plasmid was retained. After this, the cells were allowed to recover and grow with daily medium changes followed by single colony picking. Finally, a complete gene editing-free Bcl-2 KO hiPSC line was obtained due to PiggyBac excision and FIAU selection. Once the colonies were amplified, genomic DNA was collected in order to screen for the absence of the selection cassette, modification in the *BCL2* gene and potential off-target genomic insertions/modifications (see Supplemental table 2).

Genomic DNA isolation

Genomic DNA was isolated using a PureLink™ Genomic DNA Mini Kit (Invitrogen) according to the manufacturers protocol. The primers utilized for the subsequent PCR reactions can be found in Supplemental table S2. Sequencing of the PCR samples was performed by LGC genomics.

Immunoblot analysis

Cell pellets collected at 0, 7, 14 and 21 days of differentiation were resuspended on ice in lysis buffer (20 mM Tris HCl, pH7.5, 150 mM NaCl, 1.5 mM $MgCl_2$, 0.5 mM DTT, 1% Triton X-100 containing both

protease (EDTA free protease inhibitors, Thermo Fisher Scientific) and phosphatase (PhosSTOP, Roche) inhibitors), followed by further homogenizing using an eppendorf douncer in order to facilitate lysis. Lysis was performed for at least 30 min with head over end mixing at 4°C followed by centrifugation for 5 min at 4°C at >5000 xg. The supernatant was collected and protein concentration determined using a standard Bradford assay. Immunoblot samples were prepared at 0.5 µg/µl and were resolved by SDS-PAGE on 4-12% Bis Tris gradient gels (ThermoFisher) and transferred to 0.45 µm PVDF (Merck) as described in (Vervliet et al., 2014). Following this primary antibody staining was performed over night at 4°C and secondary antibody staining with HRP conjugated antibodies (Bioke) was performed at room temperature for at least 2 h. Immunoreactive bands were visualized using Pierce™ ECL Western Blotting Substrate (Thermo Fisher Scientific) and imaged using a ChemiDoc™ MP imaging system (BioRad). When the phosphorylation status of a protein was studied the phospho-specific antibody was applied first. Prior to staining the total protein fraction on the same membrane. When required, the membranes were stripped utilizing the ReBlot Plus antibody stripping solution (Merck) according to the manufacturers' instructions. The full length immunoblots merged with their colorimetric image can be found in the supplemental figures of this paper.

Quantitative reverse transcription PCR (RT-qPCR)

RNA isolation was performed using a GenElute™ mammalian total RNA miniprep kit (Sigma) according to the manufacturers protocol. After this, a DNA-free™ kit (Invitrogen) was used according to the manufacturers protocols to remove potential contaminating genomic DNA. RNA concentrations were determined using a Nanodrop. cDNA was prepared by reverse transcription from 1000 ng total mRNA using the High Capacity cDNA reverse transcription kit (Applied Biosystems). For qPCR, forward and reverse primers for the genes of interest (see Supplemental table S3) were mixed with FastStart Universal SYBR Green Master (Rox; Roche). 5 µl of this mixture was pipetted in duplicate per condition in a 384 well plate after which which 5 µl of a 1:10 dilution of the prepared cDNAs were added. Reactions were performed using a ViiA7 Real-Time PCR System (Thermo Fisher Scientific). For analysis, ΔΔCT values were determined for each condition using *GAPDH* and *RPL13a* as reference genes.

Immunofluorescence staining

Control and Bcl-2 KO cardiomyocytes were stained for cTnT after 14 days of differentiation and for c-Myc and cTnT after 7 days of differentiation. Briefly, the cells were fixed with 4% paraformaldehyde (PFA) for 10 min followed by permeabilization with 0.2% Triton X-100 in PBS containing 1% bovine

serum albumin (BSA) for 15 min. Blocking of non-specific protein binding sites was performed for 1 h in 10% goat serum. Next, the cells were incubated overnight at 4°C with c-Myc and/or cTnT antibody followed by the appropriate Alexa-555 and/or Alexa-488 conjugated secondary antibody (Thermo Fisher Scientific; 4 μg/mL) for 1 h at 37°C. Confocal images were captured using a a 63x 1.4 NA oil immersion objective on a Zeiss LSM510 confocal microscope when cells were stained for cTnT alone. When imaging the co-staining of cTnT and c-Myc, a DAPI stain was also included in order to visualize the nuclei. Herein addition, confocal images were taken using a 63x 1.4NA oil objective on a Zeiss LSM880 AxioObserver confocal microscope. All microscope settings were kept identical when acquiring these images. Quantification of cTnT signal at day 14 of differentiation was performed using FIJI software. First, the background was subtracted. Next, the threshold for cTnT staining was determined on the control condition which was utilized for all other conditions. After applying the threshold, the average intensity of the cTnT signal was measured focussing only on the cTnT positive parts of each image. Quantification of the nuclear c-Myc signal at day 7 of differentiation was performed as follows. The images were converted into tiff format with separated channels. Nuclei were identified using Stardist (Weigert et al., 2020). Pyknotic nuclei were discarded based on size and shape features for all the image sets. Cellprofiler was used to analyse the differences in the intensity and area of c-Myc signal inside the nuclei (Stirling et al., 2021). To calculate intensities, background was subtracted from the c-Myc channel based on the lower-quartile-intensity of each image from *MeasureImageIntensity* module, and mean intensities per nuclei were calculated with *MeasureObjectIntensity* module in cellprofiler. To calculate area, the c-Myc was first identified as Objects with Adaptive-threshold settings and typical diameter of objects set to 1-5px, then they were converted to b/w images using *ConvertObjectsToImage* module. The Area was finally calculated using *MeasureObjectIntensity* module to find the mean area of c-Myc per nuclei.

Intracellular Ca^{2+} imaging

Intracellular Ca^{2+} measurements were performed in hiPSC-derived cardiomyocytes differentiated for 9 or 11 days. In these experiments, cells were loaded with 1 µM of the Ca^{2+} reporter Fluo-4 AM (solubilized in cardiomyocyte maintenance medium) for 45 min in a humidified incubator at 37°C and 5% CO_2. Next, the cells were washed twice with cardiomyocyte maintenance medium, after which the dye was de-esterified for 45 min under the same conditions as for loading. Immediately prior to starting the Ca^{2+} imaging experiments, the maintenance medium was replaced with a pre-warmed (37°C) modified Krebs-Ringer solution (135 mM NaCl, 6.2 mM KCl, 1.2 mM $MgCl_2$, 12 mM HEPES, pH 7.3, 11.5 mM glucose and 2 mM $CaCl_2$). Additions were performed as indicated in the figure. Tetracaine was solubilized in the above modified Krebs-Ringer solution at 1 mM final concentration.

Imaging was performed using a Nikon eclipse Ti2 inverted fluorescence microscope (Nikon) equipped with excitation filter FF01-378/474/554/635 and dichroic mirror FF01-432/515/595/730 and emission filter 515/30, all from Semrock. Excitation was performed at 470 nm using a CoolLed pR-4000 (CoolLed). Acquisition of the emitted fluorescent signal was performed at 10 Hz using a pco.edge 4.2bi sCMOS camera (pCO). For image analysis, FIJI software (Rueden et al., 2017) was utilized. To visualise fluorescence changes, a pseudo-line scan was first generated by re-slicing of the image stack at the location of a straight line that was drawn from top to bottom over the largest area of active hiPSC-derived cardiomyocytes. Profiles of fluorescence intensity were plotted and measured as indicated in the figures. To normalise for baseline fluorescence, traces are shown as F/F0 where the F0 value was obtained during the quiescent period after tetracaine administration. To determine the area of cells showing spontaneous Ca^{2+} activity, maximum intensity Z projections were performed of the first 300 images per stack. A threshold for response was determined for one control condition in each experiment and applied to all other stacks. After thresholding, particle analyses were performed to determine the regions of interest from which the size of the areas were calculated.

Cell death measurements

Cell death measurements were performed on hiPSC-derived cardiomyocytes differentiated for 0, 7, 14 and 21 days. 15 minutes before imaging the cells were treated with a cell permeable Hoechst stain (2 µg/ml) (Merck), NuncView®488 Biotium (1 µM) (Fremont, CA, USA) and propidium iodide (1 µg/ml) (Merck) in a modified Krebs-Ringer solution (135 mM NaCl, 6.2 mM KCl, 1.2 mM $MgCl_2$, 12 mM HEPES, pH 7.3, 11.5 mM glucose and 2 mM $CaCl_2$). For each experiment a control differentiation was treated for 5 hours with 1 µM staurosporine (Tocris, Abingdon, UK) as positive control for cell death induction. Imaging was performed using the above-mentioned Nikon eclipse Ti2 inverted fluorescence microscope (Nikon). For each image excitation was performed consecutively at 360, 470 and 550 nM for Hoechst, NunCView®488 and propidium iodide respectively. Microscope settings were kept the same on each experimental day. Quantification was performed using the FIJI software. Each experimental day, the staurosporine treated condition was utilized to determine the threshold for positive NuncView®488 and propidium iodide signal. Next, this threshold was applied to all other images and the number of NuncView®488 and/or propridium iodide positive nuclei were determined relative to the total number of nuclei given by the Hoechst stain.

Statistical analysis

Statistical analysis was performed using GraphPad Prism software (Version 9.1.1). All datasets were tested for normal distribution using Shapiro-Wilk tests. For normally distributed data sets showing insignificant variability between the conditions, ANOVA tests were performed. Non-normally distributed data sets were analysed using non-parametric Kruskall Wallis tests. Additonal information on the performed statistical tests can be found in the figure legends. If not otherwise specified, p values < 0.05 were considered significant (with $p<0.05$, $p<0.01$, $p<0.001$ and $p<0.0001$ are designated as *, **, *** and **** respectively).

Acknowledgments

This work was supported by the Research Foundation-Flanders (FWO) “krediet aan navorsers” (grant number: 1508319N). TV is a recipient of a senior post-doctoral grant of the FWO (grant number: 12ZG121N). The use of the Zeiss LSM 880 – Airyscan microscope at the Cell and Tissue Imaging Cluster, was supported by Hercules AKUL/15/37_GOH1816N and FWO G.0929.15 to Pieter Vanden Berghe, University of Leuven. RD was supported by KU Leuven Rondoufonds voor Duchenne Onderzoek (EQQ-FODUCH-O2010) and KU Leuven Postdoctoral Mandate Type 1 (PDMT1/21/037).

Author contributions

Conceptualization: TV; methodology: TV, RD; investigation: TV, RD, AP and RLR; writing: TV, RD, LR, MS, AP; funding acquisition: TV and MS; supervision TV, LR and MS.

Conflict of interest

The authors declare no competing interests.

References

Aouadi, M., Bost, F., Caron, L., Laurent, K., Le Marchand Brustel, Y. & Binetruy, B. (2006). p38 mitogen-activated protein kinase activity commits embryonic stem cells to either neurogenesis or cardiomyogenesis. *Stem Cells,* **24,** 1399-406.

Blagosklonny, M. V. (2001). Unwinding the loop of Bcl-2 phosphorylation. *Leukemia,* **15,** 869-74.

Brunelle, J. K. & Letai, A. (2009). Control of mitochondrial apoptosis by the Bcl-2 family. *J Cell Sci,* **122,** 437-41.

Bywater, M. J., Burkhart, D. L., Straube, J., Sabo, A., Pendino, V., Hudson, J. E., Quaife-Ryan, G. A., Porrello, E. R., Rae, J., Parton, R. G., Kress, T. R., Amati, B., Littlewood, T. D., Evan, G. I. & Wilson, C. H. (2020). Reactivation of Myc transcription in the mouse heart unlocks its proliferative capacity. *Nat Commun,* **11,** 1827.

Chu, V. T., Weber, T., Wefers, B., Wurst, W., Sander, S., Rajewsky, K. & Kuhn, R. (2015). Increasing the efficiency of homology-directed repair for CRISPR-Cas9-induced precise gene editing in mammalian cells. *Nat Biotechnol,* **33,** 543-8.

De Chiara, G., Marcocci, M. E., Torcia, M., Lucibello, M., Rosini, P., Bonini, P., Higashimoto, Y., Damonte, G., Armirotti, A., Amodei, S., Palamara, A. T., Russo, T., Garaci, E. & Cozzolino, F. (2006). Bcl-2 Phosphorylation by p38 MAPK: identification of target sites and biologic consequences. *J Biol Chem,* **281,** 21353-21361.

Deng, X., Ruvolo, P., Carr, B. & May, W. S., Jr. (2000). Survival function of ERK1/2 as IL-3-activated, staurosporine-resistant Bcl2 kinases. *Proc Natl Acad Sci U S A,* **97,** 1578-83.

Engel, F. B., Schebesta, M., Duong, M. T., Lu, G., Ren, S., Madwed, J. B., Jiang, H., Wang, Y. & Keating, M. T. (2005). p38 MAP kinase inhibition enables proliferation of adult mammalian cardiomyocytes. *Genes Dev,* **19,** 1175-87.

Jackson, T., Allard, M. F., Sreenan, C. M., Doss, L. K., Bishop, S. P. & Swain, J. L. (1990). The c-myc proto-oncogene regulates cardiac development in transgenic mice. *Mol Cell Biol,* **10,** 3709-16.

Jin, Z., Gao, F., Flagg, T. & Deng, X. (2004). Tobacco-specific nitrosamine 4-(methylnitrosamino)-1-(3-pyridyl)-1-butanone promotes functional cooperation of Bcl2 and c-Myc through phosphorylation in regulating cell survival and proliferation. *J Biol Chem,* **279,** 40209-19.

Jin, Z., May, W. S., Gao, F., Flagg, T. & Deng, X. (2006). Bcl2 suppresses DNA repair by enhancing c-Myc transcriptional activity. *J Biol Chem,* **281,** 14446-56.

Kobayashi, S., Lackey, T., Huang, Y., Bisping, E., Pu, W. T., Boxer, L. M. & Liang, Q. (2006). Transcription factor gata4 regulates cardiac BCL2 gene expression in vitro and in vivo. *FASEB J,* **20,** 800-2.

Liang, Y., Mirnics, Z. K., Yan, C., Nylander, K. D. & Schor, N. F. (2003). Bcl-2 mediates induction of neural differentiation. *Oncogene,* **22,** 5515-8.

Limana, F., Urbanek, K., Chimenti, S., Quaini, F., Leri, A., Kajstura, J., Nadal-Ginard, B., Izumo, S. & Anversa, P. (2002). bcl-2 overexpression promotes myocyte proliferation. *Proc Natl Acad Sci U S A,* **99,** 6257-62.

Maundrell, K., Antonsson, B., Magnenat, E., Camps, M., Muda, M., Chabert, C., Gillieron, C., Boschert, U., Vial-Knecht, E., Martinou, J. C. & Arkinstall, S. (1997). Bcl-2 undergoes phosphorylation by c-Jun N-terminal kinase/stress-activated protein kinases in the presence of the constitutively active GTP-binding protein Rac1. *J Biol Chem,* **272,** 25238-42.

Patel, J. H., Loboda, A. P., Showe, M. K., Showe, L. C. & McMahon, S. B. (2004). Analysis of genomic targets reveals complex functions of MYC. *Nat Rev Cancer,* **4,** 562-8.

Pattingre, S., Tassa, A., Qu, X., Garuti, R., Liang, X. H., Mizushima, N., Packer, M., Schneider, M. D. & Levine, B. (2005). Bcl-2 antiapoptotic proteins inhibit Beclin 1-dependent autophagy. *Cell,* **122,** 927-39.

Romero-Becerra, R., Santamans, A. M., Folgueira, C. & Sabio, G. (2020). p38 MAPK Pathway in the Heart: New Insights in Health and Disease. *Int J Mol Sci,* **21**.

Rong, Y. P., Aromolaran, A. S., Bultynck, G., Zhong, F., Li, X., McColl, K., Matsuyama, S., Herlitze, S., Roderick, H. L., Bootman, M. D., Mignery, G. A., Parys, J. B., De Smedt, H. & Distelhorst, C. W. (2008). Targeting Bcl-2-IP_3 receptor interaction to reverse Bcl-2's inhibition of apoptotic calcium signals. *Mol Cell,* **31,** 255-65.

Rueden, C. T., Schindelin, J., Hiner, M. C., DeZonia, B. E., Walter, A. E., Arena, E. T. & Eliceiri, K. W. (2017). ImageJ2: ImageJ for the next generation of scientific image data. *BMC Bioinformatics,* **18,** 529.

Stirling, D. R., Swain-Bowden, M. J., Lucas, A. M., Carpenter, A. E., Cimini, B. A. & Goodman, A. (2021). CellProfiler 4: improvements in speed, utility and usability. *Bmc Bioinformatics,* **22**.

Veis, D. J., Sorenson, C. M., Shutter, J. R. & Korsmeyer, S. J. (1993). Bcl-2-deficient mice demonstrate fulminant lymphoid apoptosis, polycystic kidneys, and hypopigmented hair. *Cell,* **75,** 229-40.

Vervliet, T., Decrock, E., Molgo, J., Sorrentino, V., Missiaen, L., Leybaert, L., De Smedt, H., Kasri, N. N., Parys, J. B. & Bultynck, G. (2014). Bcl-2 binds to and inhibits ryanodine receptors. *J Cell Sci,* **127,** 2782-92.

Vervliet, T., Parys, J. B. & Bultynck, G. (2016). Bcl-2 proteins and calcium signaling: complexity beneath the surface. *Oncogene,* **35,** 5079-92.

Wei, L., Cui, L., Snider, B. J., Rivkin, M., Yu, S. S., Lee, C. S., Adams, L. D., Gottlieb, D. I., Johnson, E. M., Jr., Yu, S. P. & Choi, D. W. (2005). Transplantation of embryonic stem cells overexpressing Bcl-2 promotes functional recovery after transient cerebral ischemia. *Neurobiol Dis,* **19,** 183-93.

Weigert, M., Schmidt, U., Haase, R., Sugawara, K. & Myers, G. (2020). Star-convex Polyhedra for 3D Object Detection and Segmentation in Microscopy. *2020 Ieee Winter Conference on Applications of Computer Vision (Wacv)***,** 3655-3662.

Zhou, M., Zhang, Q., Zhao, J., Liao, M., Wen, S. & Yang, M. (2017). Phosphorylation of Bcl-2 plays an important role in glycochenodeoxycholate-induced survival and chemoresistance in HCC. *Oncol Rep,* **38,** 1742-1750.

Figures

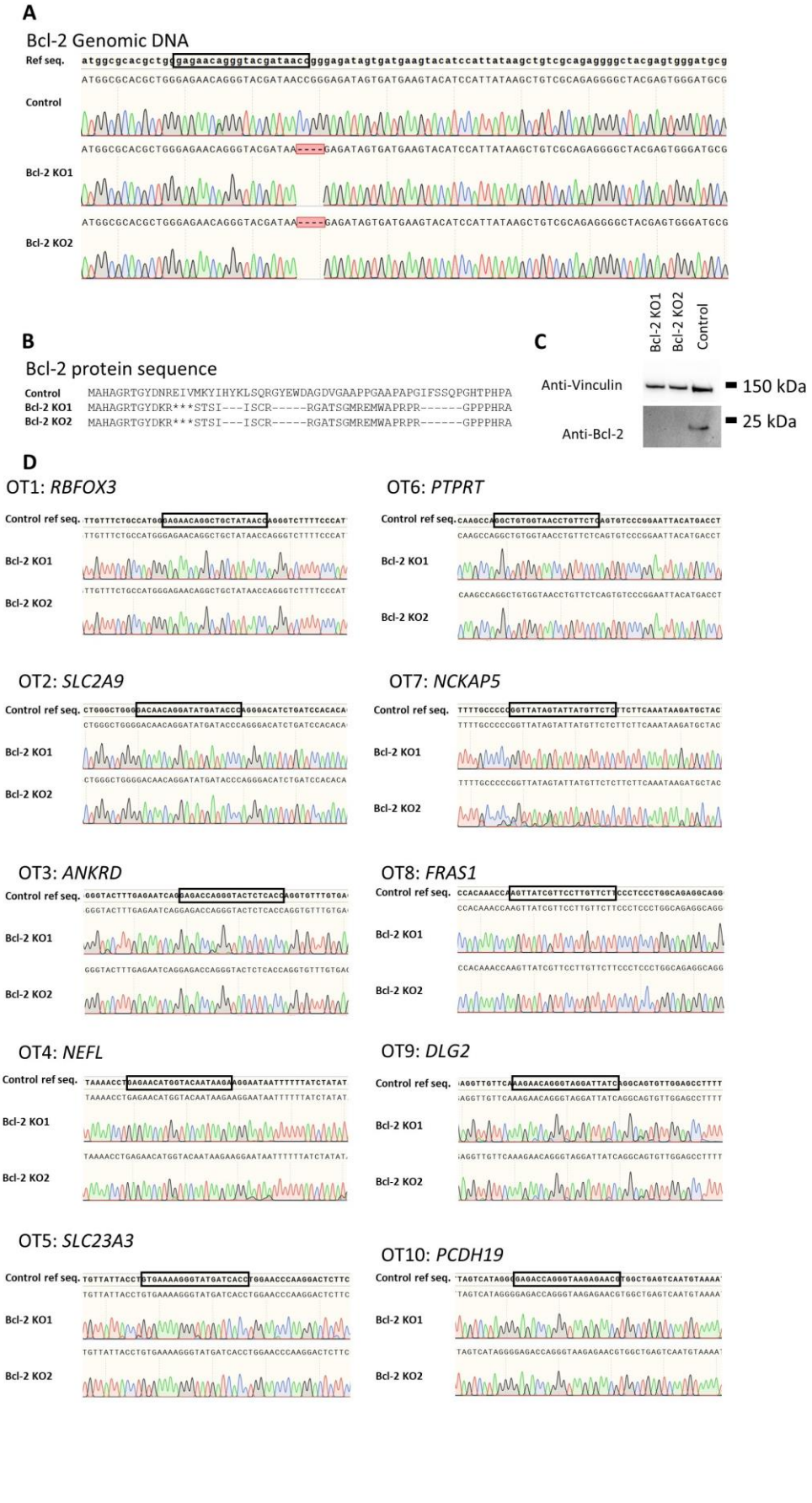

Fig. 1. CRISPR/Cas9-mediated KO of Bcl-2 in hiPSC

A) Sanger sequencing of the first 100 base pairs of the genomic Bcl-2 open reading frame comparing the sequence of the control condition to the two Bcl-2 KO hiPSC clones utilized in this study. The utilized sgRNA is indicated by the black box in the *BCL2* reference sequence (ref seq.). **B)** Predicted protein sequence based on the sequencing result obtained in A for the control and Bcl-2 KO hiPSC. * indicates the presence of a premature stop codons. **C**) Immunoblot validating the absence of Bcl-2 in the Bcl-2 KO clones compared to the control. **D**) Sequencing results surrounding the 10 most likely off-target genes associated with the utilized sgRNA. The potential off-target is indicated by the black box in the ref seq. All DNA sequences and profiles were visualized using SnapGene® software.

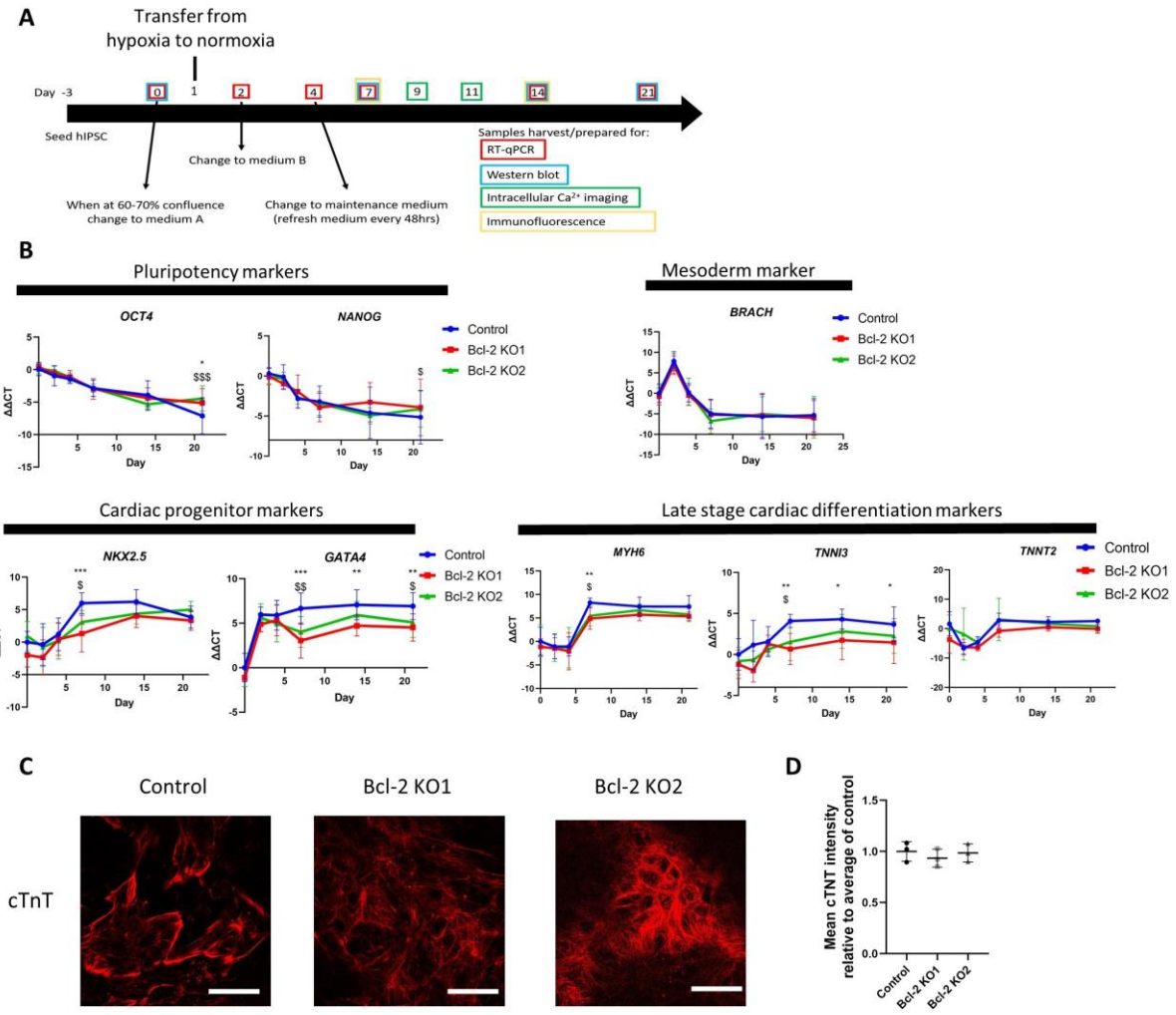

Fig. 2. Bcl-2 KO delays the expression of certain cardiac differentiation markers

A) Scheme of the cardiac differentiation protocol and time points where samples were harvested for RT-qPCR, immunoblot, immunofluorescence staining or utilized for intracellular Ca^{2+} imaging. **B)** RT-qPCR analysis of gene expression profile associated with cardiomyocyte differentiation in control and the two Bcl-2 KO clones at time points shown (0, 2, 4, 7 14, 21 days of differentiation). The data points represent ΔΔCT ± SD values of at least 4 independent differentiations (n≥4) of the indicated genes at the indicated time points. Two-way ANOVA tests with Dunnet-post test for multiple comparison were performed. * and $ indicate significant difference between control and Bcl-2 KO1 or Bcl-2 KO2 respectively * or $ indicates p<0.05, ** or $$ indicates p<0.01, *** or $$$ indicate p<0.001. **C)** Confocal images of control and Bcl-2 KO cardiomyocytes differentiated for 14 days immunofluorescently stained for cTnT. Experiments were performed 3 times independently (n=3). The white scale bar corresponds to 50 µM. **D)** Quantification of the cTnT signal of the

immunofluorescence experiments, comparing control to the Bcl-2 KO lines. Data points depict the averaged cTnT intensity from all pictures acquired from one independent experiment, relative to the average of the control conditions across all experiments. In total three independent experiments were performed (n=3). No significant differences were detected between the conditions after ANOVA testing.

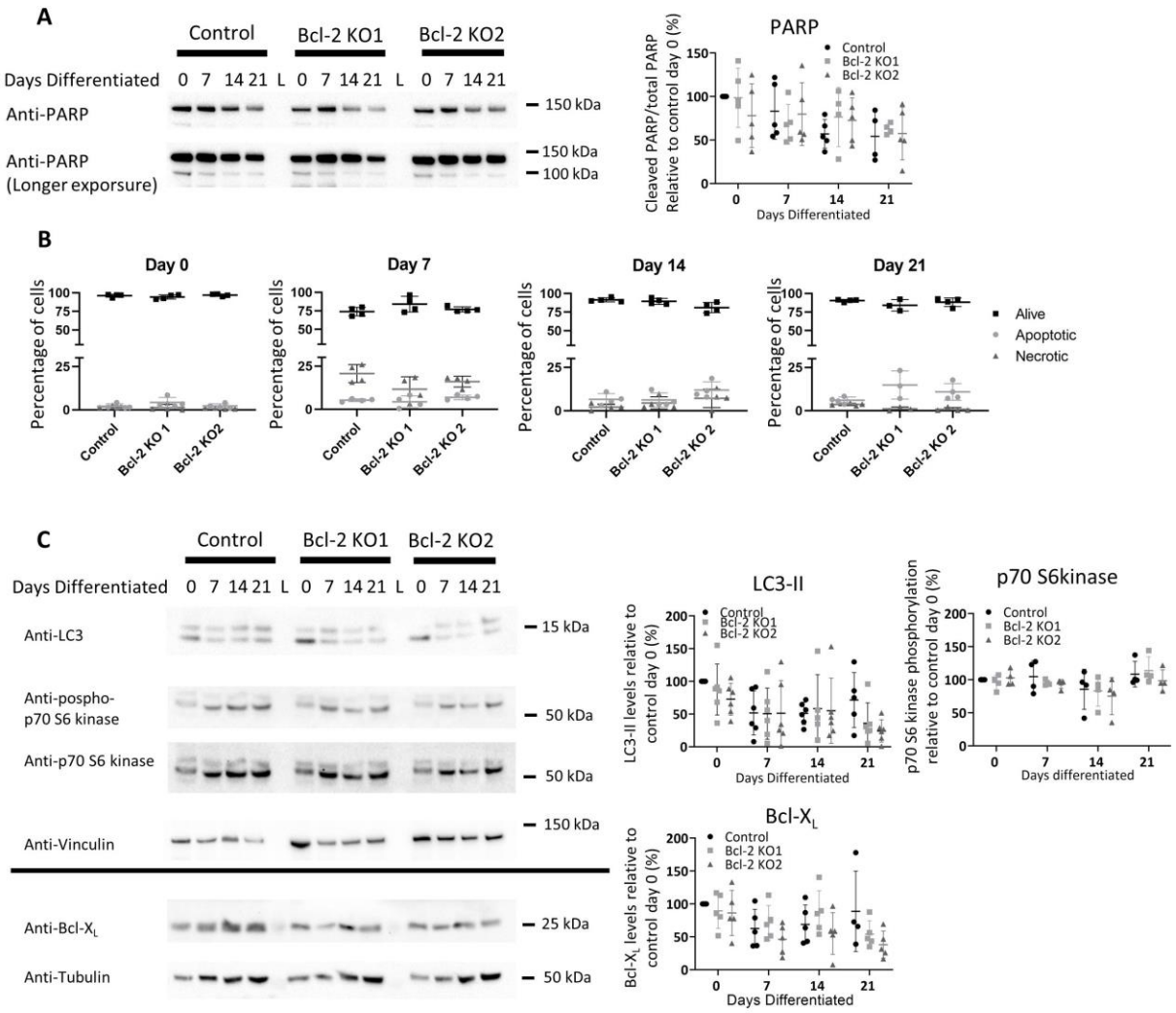

Fig. 3. Basal levels of apoptosis, necrosis and autophagy induction are unaltered upon KO of Bcl-2

A) immunoblot analysis for the indicated proteins in lysates prepared from cardiomyocytes derived from control or Bcl-2 KO clones differentiated for 0, 7, 14 or 21 days (*left panel)*. L depicts the lane in which molecular weight ladders were loaded. **Q**uantification of the performed immunoblot experiments *(right panel)*. The expression levels of cleaved PARP were normalised to the total PARP levels. All protein levels are shown relative to the levels for control day 0. All differentiations were performed at least 4 times (n≥4) the average ± SD is indicated in the figures. For comparing day 0 values, a non-parametric Kruskall-Wallis tests with Dunn/s multiple comparison was performed to compare to the normalized control value of control day 0. For all other days, one-way ANOVA tests with Tukey-post test for multiple comparison were performed as the assumptions of normality were met in these conditions. **B)** Quantification of the performed cell death experiments after 0, 7, 14 and 21 days of differentiation of control and Bcl-2 KO clones. 15 minutes before image acquisition the cells were co-treated with a cell permeable Hoechst stain, NucVIEW®488 and propidium iodide. Cells positive for either NucView®488 or both NucView®488 and propidium iodide were identified as

apoptotic. Cells only positive for propidium iodide were classified as necrotic. All values were normalized to the total cell count obtained by the cell permeable Hoechst stain. The experiment was performed at least 3 times independently (n≥3). ANOVA tests with Tukey-post test for multiple comparison were performed as the assumptions of normality were met in all conditions. No significant differences were detected. **C)** Immunoblot analysis for the indicated proteins in lysates prepared from cardiomyocytes derived from control or Bcl-2 KO clones differentiated for 0, 7, 14 or 21 days *(left panels)*. The black horizontal line depicts which immunostainings were performed on the same immunoblot. L depicts the lane in which molecular weight ladders were loaded. For p70 S6 kinase activity, the phosphorylated p70 S6 kinase levels were divided by the total p70 S6kinase levels. All other protein expression levels are plotted normalized to their corresponding loading control ran on the same immunoblot (vinculin or tubulin). All protein levels are shown relative to the levels for control day 0 *(right panels)*. All differentiations were performed at least 4 times (n≥4) the average ±SD is indicated in the figures. For comparing day 0 values, a non-parametric Kruskall-Wallis tests with Dunn's multiple comparison was performed to compare to the normalized control value of control day 0. For all other days, one-way ANOVA tests with Tukey-post test for multiple comparison were performed as the assumptions of normality were met in these conditions.

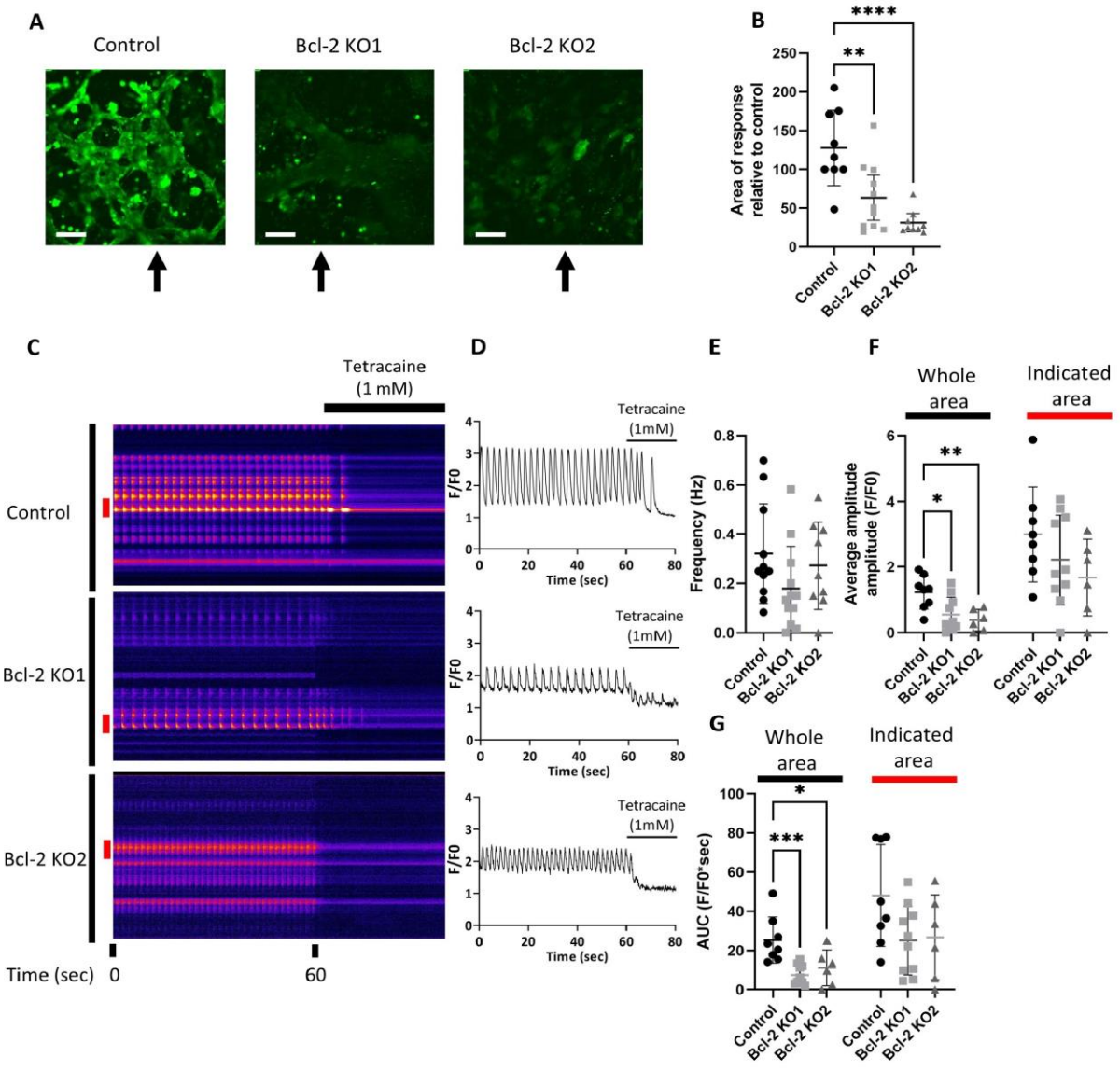

Fig. 4. KO of Bcl-2 reduces the area of spontaneous activity as well as the spontaneous Ca^{2+} release

Spontaneous intracellular Ca^{2+} measurements in cardiomyocytes differentiated for 9 or 11 days using Fluo-4. **A)** Maximum intensity projections of the first 30 s (300 images) of a representative Ca^{2+} measurement for control and Bcl-2 KO conditions. The white scale bar corresponds to 100 µM. The arrows indicate where the line was drawn for "reslicing" the stack in **C**. **B)** Quantification of the area of spontaneous activity derived from the maximum intensity plots relative to the total area covered by cells (%). Each data point represents the size of the area of spontaneous activity of a single Ca^{2+} imaging experiment. The average ± SD are indicated on the graphs. The experiment was performed at least 9 times independently for each condition (n≥9). **C)** Visual representation of the experiment showing a time laps of the pseudo-line scans obtained after re-slicing the image stack for control and Bcl-2 KO conditions. After 60 s, tetracaine (1 mM) was added to block RyR activity and determine the baseline **D)** Intensity profiles obtained by quantifying the entire area (indicated by the black bar left

of the pseudo-line scans in **C**) plotted as F/F0. F0 was determined after tetracaine addition. Quantification of the spontaneous activity was obtained by determining the frequency **(E)**, amplitude **(F)** and area under the curve **(G)**. For amplitude and frequency an additional quantification was performed focussing only on the areas of most intense responses (indicated by the red bar left of the line scans in **C**). All experiments were performed at least 6 times ($n \geq 6$). The averages ± SD are represented on the graphs. For statistical analysis one-way ANOVA tests with Tukey-post test for multiple comparison were performed. * indicates $p<0.05$, ** indicates $p<0.01$, *** indicate $p<0.001$

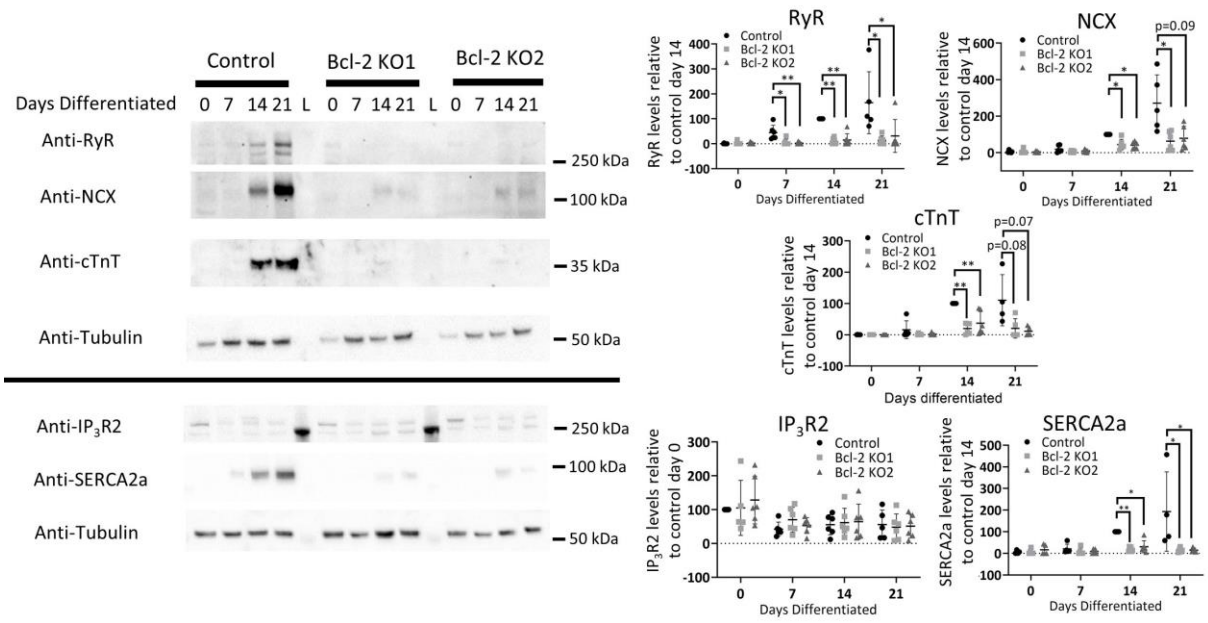

Fig. 5. KO of Bcl-2 impairs the expression of the cardiac Ca^{2+} toolkit

A) Immunoblot analysis of the indicated proteins in lysates prepared from cardiomyocytes derived from control or Bcl-2 KO clones differentiated for 0, 7, 14 or 21 days. The horizontal black line indicates which immunostainings were performed on the same immunoblot. L depicts the lane in which molecular weight ladders were loaded. **B)** quantification of the performed immunoblot experiments. All protein expression levels are normalized towards their corresponding loading control (tubulin) stained on the same membrane. All values were normalized to a control condition where expression levels were easily detected throughout the different experimental repetitions. For RyR, SERCA2a, cTnT, NCX this was control day 14 as for IP_3R2 this was control day 0. Each data point represents and independent differentiation which were performed at least 4 times (n≥4). The averages ± SD are represented on the graphs. As the assumption for normal distribution were not met for all conditions, non-parametric Kruskall-Wallis tests with Dunn's multiple comparison were performed * indicates $p<0.05$ and ** indicates $p<0.01$.

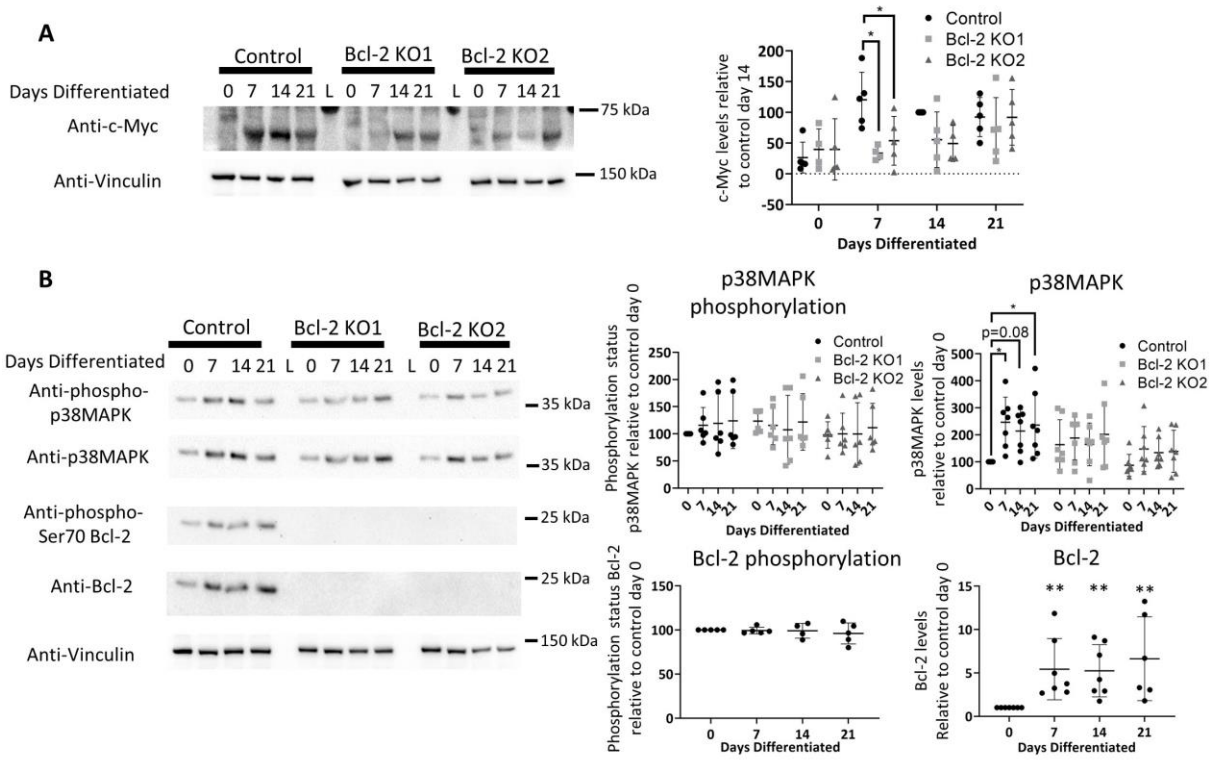

Fig. 6. Bcl-2 KO impairs upregulation of c-Myc

A,B) Left, immunoblot analysis of cardiomyocytes derived from control or Bcl-2 KO clones differentiated for 0, 7, 14 or 21 days, stained for the indicated proteins. L depicts the lane in which molecular weight ladders were loaded. **Right**, quantification of the performed immunoblot experiments. For quantifying the phosphorylation status of p38MAPK or Bcl-2, the protein levels detected by the phospho-antibody were normalized to the total amount of p38MAPK or Bcl-2. For all other quantifications, protein levels were normalized to their respective loading control (vinculin) and shown relative to a control condition were the protein was easily detected. For Bcl-2 and p38MAPK, this was control day 0 whereas for c-Myc, this was control day 14. All differentiations were performed at least 4 times independently (n≥4). The averages ± SD are represented on the graphs. In the conditions normalized to, the assumptions for normal distribution were not met. Therefore, when comparing these conditions Kruskall-Wallis tests with Dunn's multiple comparison were performed. All other conditions were normally distributed and allowed the use of one-way ANOVA tests with Tukey-post test for multiple comparison were performed. * indicates $p<0.05$, ** indicates $p<0.01$.

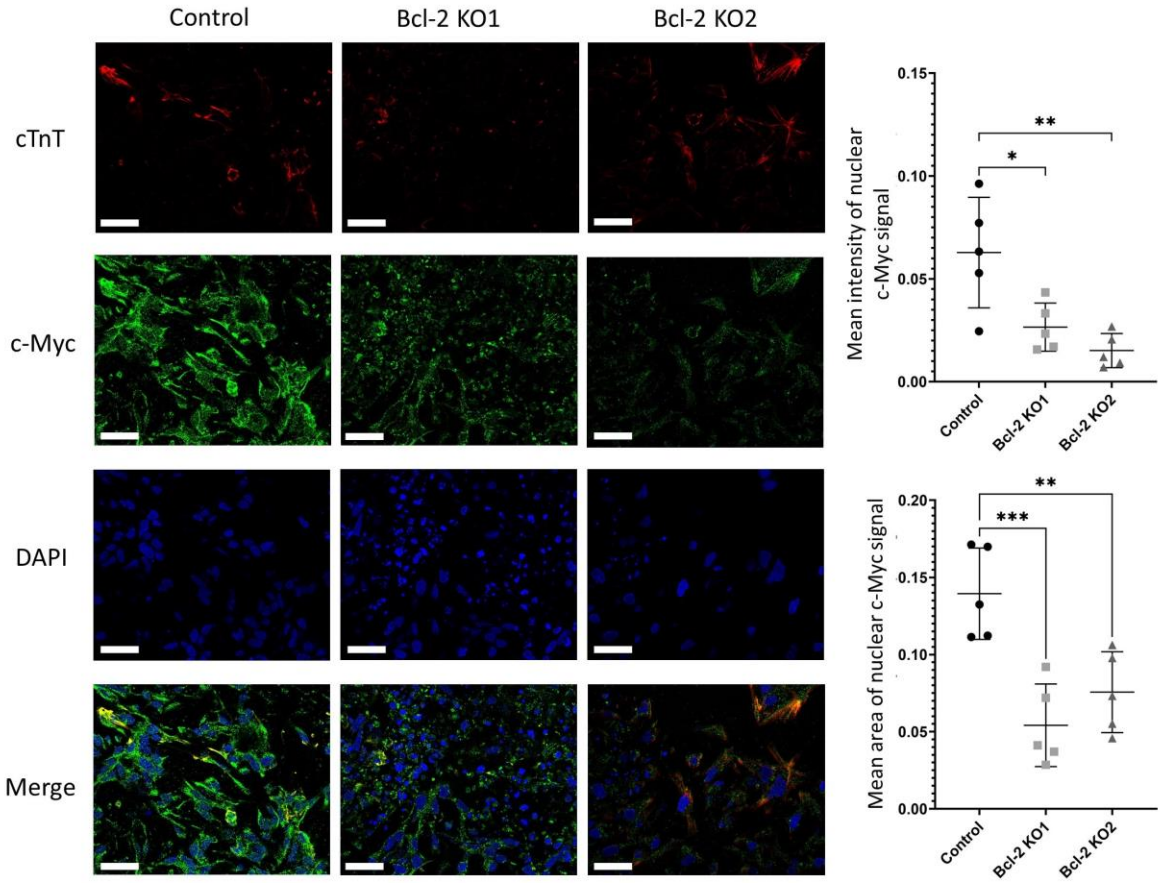

Fig. 7. KO of Bcl-2 reduces nuclear c-Myc localization

A) Confocal images of control and Bcl-2 KO cardiomyocytes differentiated for 7 days loaded with Hoechst and immunofluorescently stained for cTnT and c-Myc. The white scale bar corresponds to 20 µM **B)** Quantification of the intensity (top) and area (bottom) occupied by nuclear c-Myc. Each data point indicates the average intensity or area of the c-Myc stain of all nuclei in one experimental day. The experiments were performed 5 times independently (n=5). All conditions were normally distributed allowing the use of one-way ANOVA test with Tukey-post test for multiple comparison. * indicates $p<0.05$, ** indicates $p<0.01$.

Fig. S1

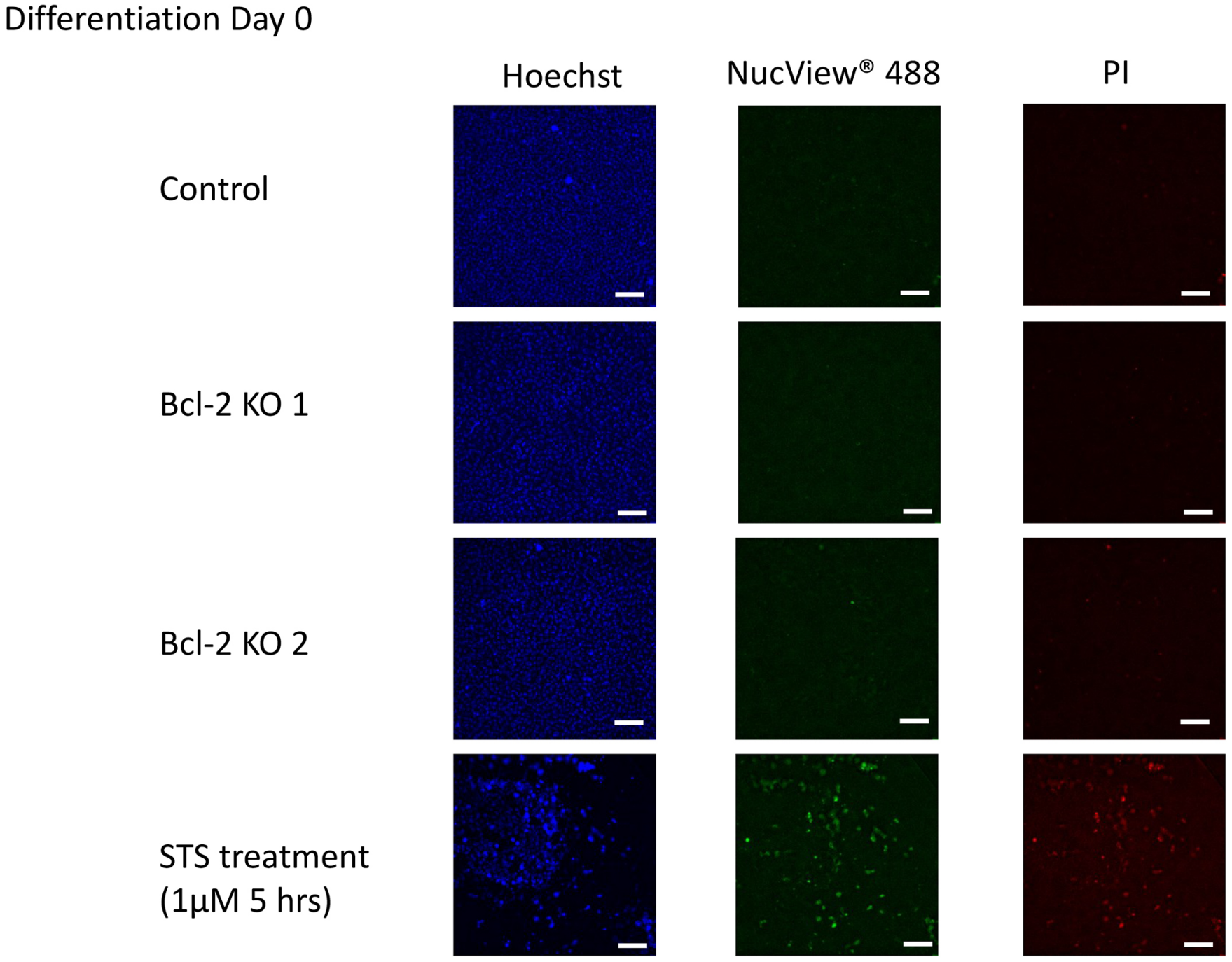

Fig. S2

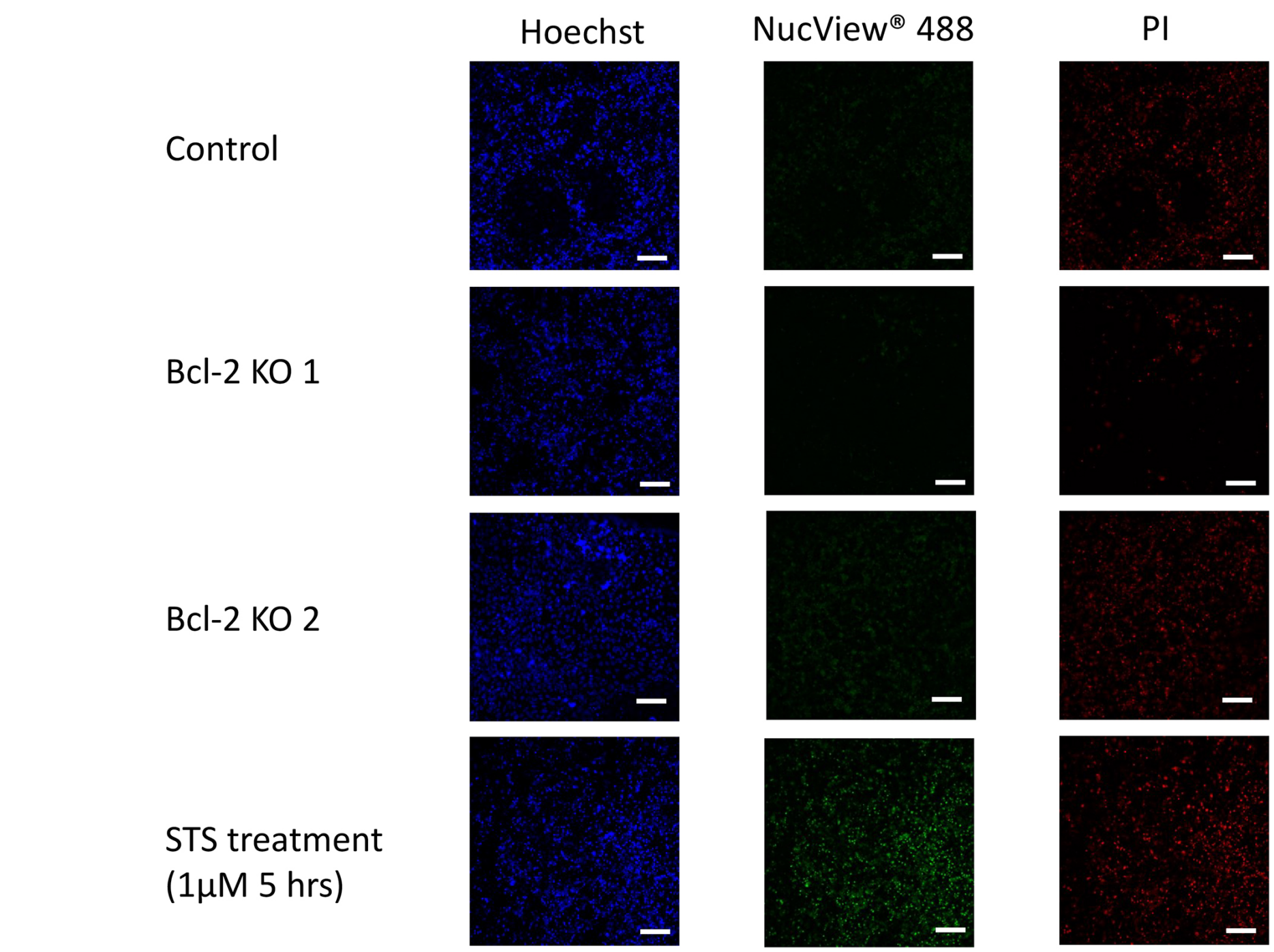

Fig. S3

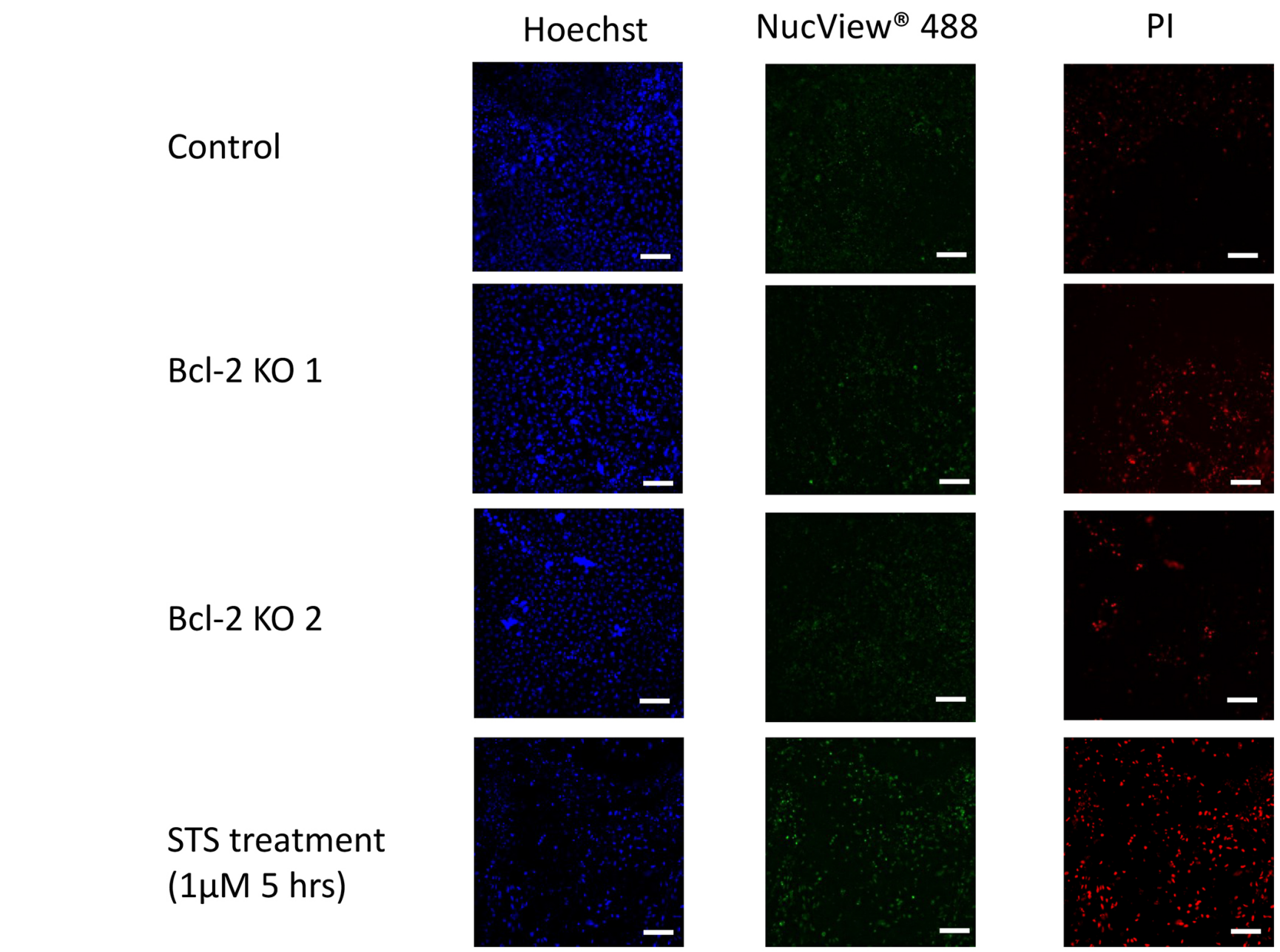

Fig. S4

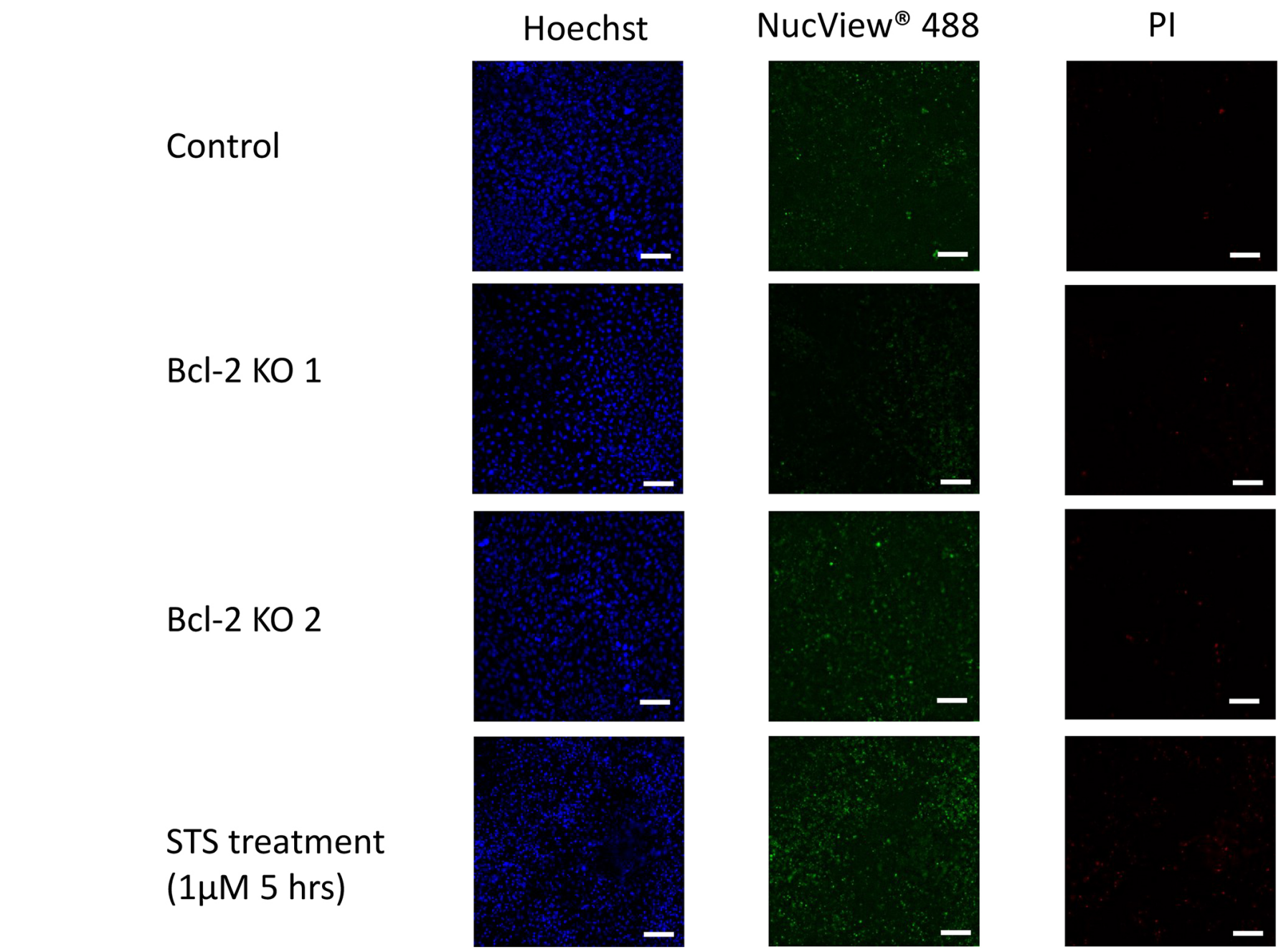

Figs. S1-S4. Cell death induction is not altered upon KO of Bcl-2. Typical images taken on differentiation day 0, 7, 14 and 21 (supplemental figure 1, 2, 3, 4 respectively) of control and Bcl-2 KO conditions. Cells were stained 15 min prior to image acquisition with a cell permeable Hoechst stain, NucView®488 and propidium iodide (PI) to monitor total nucleus count, caspase 3 activity and cell integrity respectively. Each experimental day a staurosporine treatment (1 µM for 5 hours) is taken with as positive control for the different dyes. The white scale bar corresponds to 100 µM. Quantification of these experiment can be found in figure 2B in the main manuscript file.

Table S1. Antibodies used

Name	Source	Catalog number	Dilution	Validation/reference
anti-Vinculin	Merck	#V-9131	1/5000	PMID: 20098684
anti-c-Myc	Merck	#M4439	1/2000	M4439 product page
anti-Tubulin	BD Pharmingen	#556321	1/5000	PMID: 8743943
anti-Bcl-2 HRP	Santa Cruz	#sc7382HRP	1/500	PMID: 26436418
anti-phospho Ser70-Bcl-2	Santa Cruz	#sc-293128	1/1000	PMID: 35176677
anti-phospho-p70 S6 kinase	Cell Signalling	#9234S	1/1000	PMID: 35551922
anti-p70 S6 kinase	Cell Signalling	#9202	1/1000	PMID: 36270994
anti-phospho-p38MAPK	Cell Signalling	#9215S	1/1000	PMID: 36329021
anti-p38MAPK	Cell Signalling	#9212	1/1000	PMID: 36329021
anti-Bcl-X_L	Cell Signalling	#2764	1/1000	PMID: 36289220
anti-PARP	Cell Signalling	#9532S	1/3000	PMID: 36257929
anti-LC3	Nanotools	#0231-100/LC3-5F10	1/500	PMID: 29358170
Anti-RyR (C3:33)	ThermoFisher Scientific	#MA3-916	1/1000	PMID: 23895152
anti-NCX (C2:C12)	ThermoFisher Scientific	#MA3-926	1/1000	PMID: 23511010
anti-cTnT	Abcam	#ab209813	1/2000	PMID: 33054489
anti-IP_3R2	Abiocode	#R2872-2	1/1000	R2872-2 product page
anti-SERCA2a	Dr. Wuytack (KU Leuven)		1/2000	PMID: 2244871

Table S2. List of primers used for genomic DNA screening

Gene	Primer direction	Primer sequence (5’ > 3’)
BCL2	forward	GTGCTGAAGATTGATGGGATCG
	reverse	CTCAAAGAAGGCCACAATCCTCC
HAL insertion	forward	GCGCGTCCTGCCTTCATTTATCC
	reverse	GACACTTACCGCATTGACAAGCACG
HAR insertion	forward	AGGCGGGCCATTTACCGTAAG
	reverse	GAGGAGAAGATGCCCGGTGC
RFBOX	forward	AGTCCCAGCCCTCTAATCACAAAG
	reverse	GGTGACTTTGGACAGGTGGCTCAG
SLC2A9	forward	ATTCTCACAACATCCCTGCCAGTGC
	reverse	GAAGGTGCAACACAATGACTCTGG
ANKRD28	forward	CAGACAGTGATCCTTAGGCTTC
	reverse	CACAAGGCGGAAATAGTCTGGCACC
NEFL	forward	GTTCAGGATCTACGGCAATGTG
	reverse	TGCAATGTCCAACCAGTCAAGC
SLC23A	forward	CCTAACTAATACAGCCCTCACTGG
	reverse	CCAGGCTCGGGTGAGGGAGTTAC
PTPRT	forward	AGCATTGCCAACCACTAGCAGAAG
	reverse	TGATGCGGATGAAGAGGCTGAGTC
NCKAP5	forward	GAAGGCAGGGATAGGGCAGGACAAG
	reverse	GCAAAGTGAGGAGACGAGATAACC
FRAS1	forward	AAGCACAGGACCAGACTTGCCAG
	reverse	GGCTGGCAGTTTGGAACAGGTGTG
DLG2	forward	GAGGAAATGGATGGAGAGTGAGG
	reverse	AAGCCTTCAGGGAGTGACCATC
PCDH19	forward	CAGCAATCGACTCCAAAGAACC
	reverse	TTCACTGAGCCTAACCACCAAG

Table S3. List of primers utilized in this study for Quantitative Real-Time PCR.

Gene	Primer direction	Primer sequence (5' > 3')
OCT4	forward	CGAGCAATTTGCCAAGCTCCTGAA
	reverse	GCCGCAGCTTACACATGTTCTTGA
NANOG	forward	TGGCCGAAGAATAGCAATGGTGTG
	reverse	TTCCAGGTCTGGTTGCTCCACATT
BRACH	forward	ACCCAGTTCATAGCGGTGAC
	reverse	AAGCTTTTGCAAATGGATTG
GATA4	forward	CGACACCCCAATCTCGATATG
	reverse	GTTGCACAGATAGTGACCCGT
NKX2.5	forward	ACCTCAACAGCTCCCTGACTCT
	reverse	ATAATCGCCGCCACAAACTCTCC
MYH6	forward	GCCCTTTGACATTCGCACTG
	reverse	CGGGACAAAATCTTGGCTTTGA
TNNI3	forward	GATGCGGCTAGGGAACCTC
	reverse	GCATAAGCGCGGTAGTTGGA
TNNT2	forward	ACAGAGCGGAAAAGTGGGAAG
	reverse	TCGTTGATCCTGTTTCGGAGA
GAPDH	forward	TCAAGAAGGTGGTGAAGCAGG
	reverse	ACCAGGAAATGAGCTTGACAAA
RPL13a	forward	CCTGGAGGAGAAGAGGAAAGAGA
	reverse	TTGAGGACCTCTGTGTATTTGTCAA

Table S4. *BCL2* homologues sequences used for CRISP/Cas9 approach

BCL2 homologues sequence (HAL) TGTAAATTGCCGAGAAGGGGAAAACATCACAGGACTTCTGCGAATACCGGACTGAAAATTGTAATTC ATCTGCCGCCGCCGCTGCCTTTTTTTTTTCTCGAGCTCTTGAGATCTCCGGTTGGGATTCCTGCGGA TTGACATTTCTGTGAAGCAGAAGTCTGGGAATCGATCTGGAAATCCTCCTAATTTTTACTCCCTCTC CCCGCGACTCCTGATTCATTGGGAAGTTTCAAATCAGCTATAACTGGAGAGTGCTGAAGATTGATGG GATCGTTGCCTTATGCATTTGTTTTGGTTTTACAAAAAGGAAACTTGACAGAGGATCATGCTGTACT TAAAAAATACAAGTAAGTTCTCTGCACAGGAAATTGGTTTAATGTAACTTTCAATGGAAACCTTTGA GATTTTTTACTTAAAGTGCATTCGAGTAAATTTAATTTCCAGGCAGC
BCL2 homologues sequence (HAR) TACATTCTTTTTAGCCGTGTTACTTGTAGTGTGTATGCCCTGCTTTCACTCAGTGTGTACAGGGAAA CGCACCTGATTTTTTACTTATTAGTTTGTTTTTTCTTTAACCTTTCAGCATCACAGAGGAAGTAGAC TGATATTAACAATACTTACTAATAATAACGTGCCTCATGAAATAAAGATCCGAAAGGAATTGGAATA AAAATTTCCTGCATCTCATGCCAAGGGGGAAACACCAGAATCAAGTGTTCCGCGTGATTGAAGACAC CCCCTCGTCCAAGAATGCAAAGCACATCCAATAAAATAGCTGGATTATAACTCCTCTTCTTTCTCTG GGGGCCGTGGGGTGGGAGCTGGGGCGAGAGGTGCCGTTGGCCCCCGTTGCTTTTCCTCTGGGAAGGA TGGCGTAAGCTGGGAGAACAGGGTACGATAACCGTGAGATAGTGTAAA

Supplementary full length immunoblots for figures 1, 3, 5 and 6

All immunoblots are shown merged with the colorimetric image of the actual membrane in order to visualize exactly where the membranes were cut.

Full length blots Figure 1

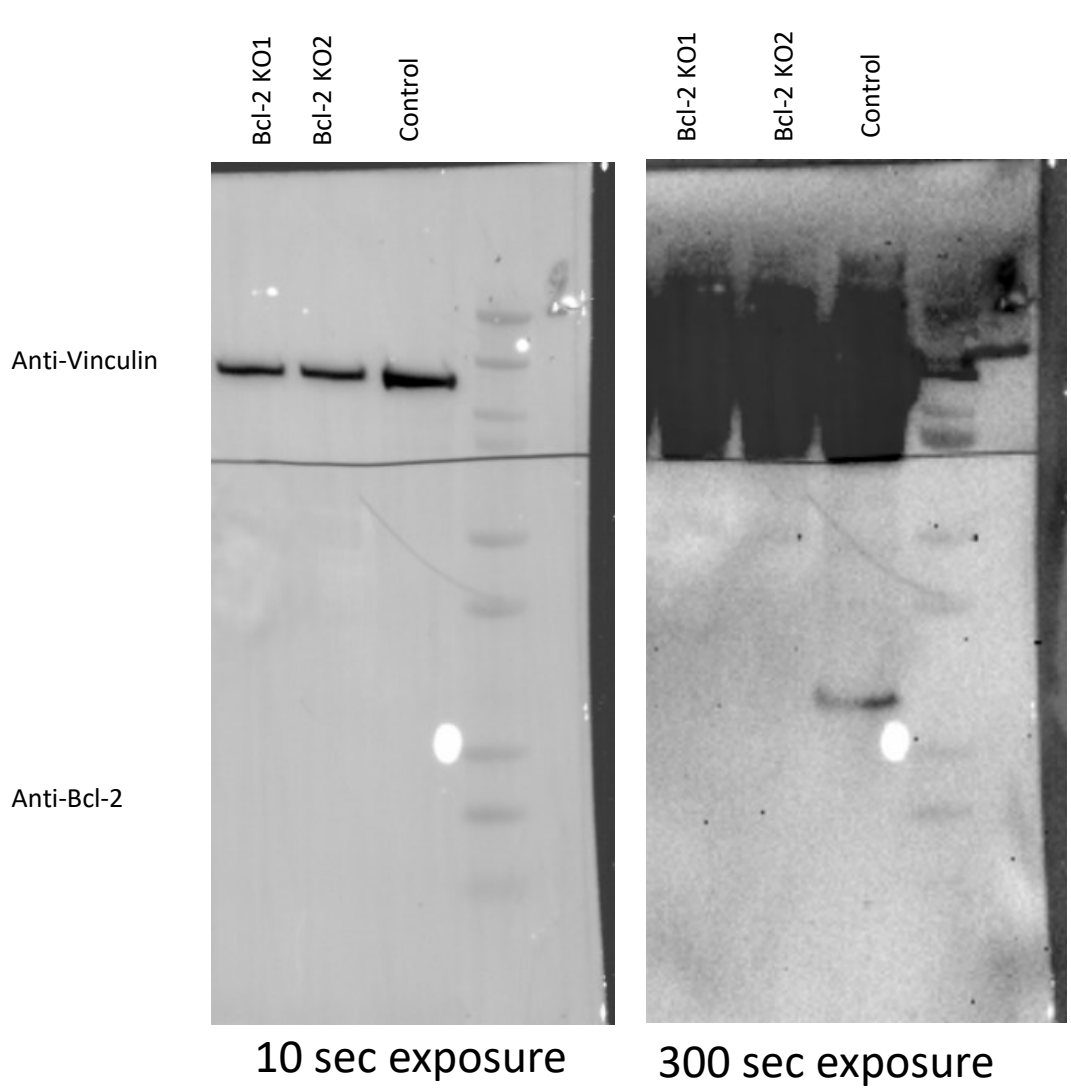

Figure 1

Full length blots Figure 3

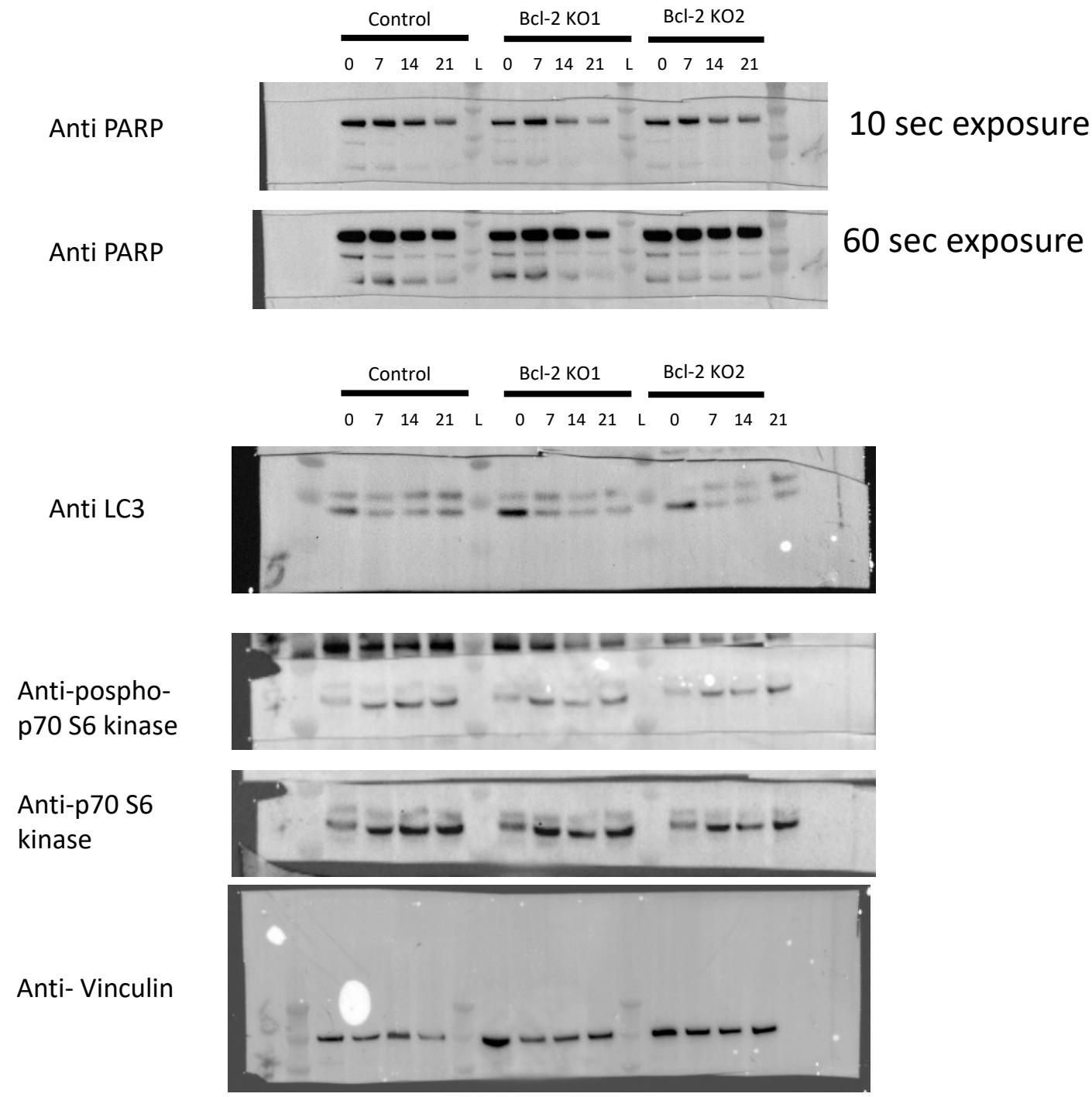

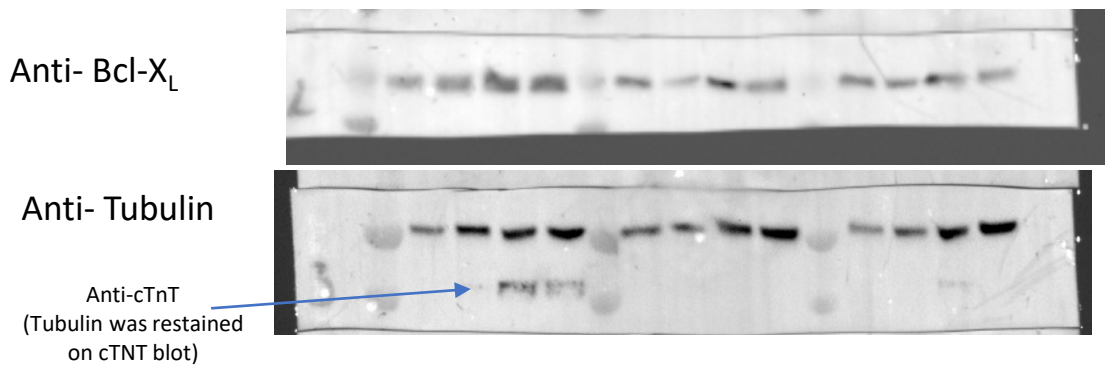

Full length blots Figure 5

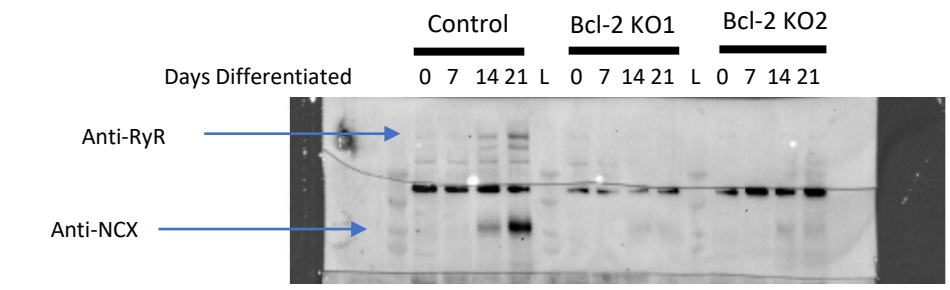

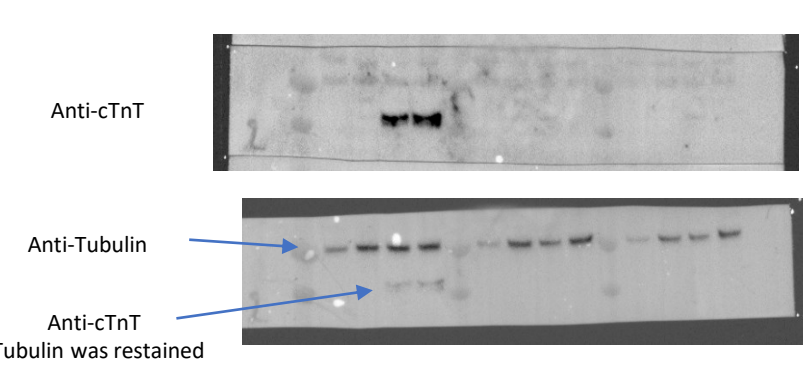

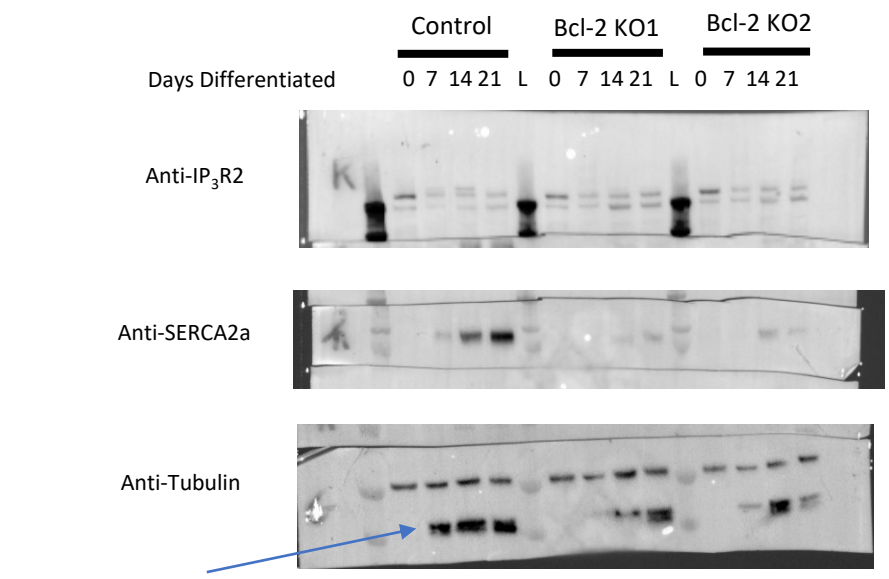

Full length blots Figure 6